Available online at www.sciencedirect.com
SCIENCE DIRECT
Lithos 89 (2006) 300–328
LITHOS
www.elsevier.com/locate/lithos

Mantle processes in an Archean orogen: Evidence from 2.67 Ga diamond-bearing lamprophyres and xenoliths

D.A. Wyman [a,*], J.A. Ayer [b], R.V. Conceição [c], R.P. Sage [b,1]

[a] *School of Geosciences, University of Sydney, Australia*
[b] *Precambrian Geoscience Section, Ontario Geological Survey, Sudbury, Ontario, Canada*
[c] *Laboratório de Geologia Isotópica, Universidade Federal do Rio Grande do Sul, Porto Alegre, Brazil*

Received 12 January 2005; accepted 23 December 2005
Available online 20 February 2006

Abstract

The world's oldest diamond deposits occur in ~2.67 Ga dikes and heterolithic breccias emplaced into greenstone belts of the Wawa and Abitibi Subprovinces, southern Superior Province, Canada. Thousands of white to yellow microdiamonds and macrodiamonds to 5 mm in width have been recovered by non-contaminating fusion techniques. The host rocks exhibit petrographic and compositional features that are characteristic of post-Archean minettes and spessartites of the calc-alkaline or shoshonitic lamprophyre clan. Based on chemical trends and petrographic evidence, host rocks that contain more than ~16 wt.% MgO represent lamprophyre magmas that entrained cumulate olivine, probably at the base of the crust. Breccia bodies that are tens of metres wide at the two localities are somewhat atypical of late Archean lamprophyre occurrences in the Superior Province and owe their size to optimum conditions for magma ascent that were required to preserve the diamonds. Abundant altered ultramafic xenoliths occur in the host rocks. The majority of xenoliths studied (10 of 14) display uniform major element compositions similar to websterite cumulate suites derived from crystal fractionation processes at the base of post-Archean volcanic arcs. The xenoliths display highly variable trace element abundances that are characteristic of cryptic metasomatism associated with the flux of an oxidised fluid above a subduction zone.

The tectonic setting of the deposits and the nature of the host rocks indicate that the diamonds may be derived from the asthenospheric wedge and subducted slab at shallow depths (100 to 160 km) rather than the deep keels of Archean cratons associated with traditional diamond deposit types. Models of low-temperature Phanerozoic diamond formation in active subduction zones, or rapid uplift and emplacement of peridotite massif occurrences, can be adapted to the Archean deposits. The stability field of diamonds in most Phanerozoic subduction scenarios, however, may be too deep to be accessed by the lamprophyric magmas. In contrast, shallow subduction, as invoked for the distinctive occurrence of adakitic (slab-melt) type rocks in the southern Superior Province, could generate two different diamond stability windows at sufficiently shallow depths to account for their presence in lamprophyric magmas.

The multiple requirements imposed on Archean tectonic models by occurrences of diamonds in hydrous shoshonitic rock types (spessartite and minette lamprophyres), along with distinctively metasomatised xenoliths, strongly favour plate tectonic subduction models of orogeny. Evidence of slightly earlier mantle plumes, such as 2.7 Ga komatiites, only strengthens the need for a subduction-driven low-temperature thermal anomaly in the Archean mantle prior to lamprophyric magmatism.

Keywords: Diamond; Archean; Lamprophyre; Shoshonite; Xenolith; Superior Province

* Corresponding author. Tel.: +61 2 9351 2924; fax: +61 2 9351 0184.
E-mail address: dwyman@geosci.usyd.edu.au (D.A. Wyman).
[1] Retired.

0024-4937/$ - see front matter © 2006 Elsevier B.V. All rights reserved.
doi:10.1016/j.lithos.2005.12.005

1. Introduction

The world's oldest diamond deposits have recently been discovered in late Archean lamprophyric dikes and diatreme breccias of Canada's Superior Province. Given the well-characterised pressure and temperature constraints on diamond formation, the occurrences are of major importance for our understanding of the Archean geotherm and tectonics at the time of diamond emplacement. This paper first compares the diamond host rocks with previously recognised Superior Province lamprophyres in order to establish whether they are members of a common igneous suite. The geodynamic significance of the deposits is then assessed in terms of diamond P–T stability requirements and the geochemical characteristics of the mantle-derived host rocks. The results are used to determine whether this new class of diamond deposit has strong affinities with any post-Archean types of diamond occurrences.

2. Diamond characteristics and regional setting

Diamonds were first discovered in situ in an Archean-aged dike at the Sandor locality in the Michipicoten greenstone belt (MGB) of the eastern Wawa Subprovince in 1996 (Sage, 2000). Additional occurrences were subsequently identified at several nearby localities in the MGB and another occurrence was identified in lamprophyric dike and breccia of Lorrain Township near the town of Cobalt in the western Abitibi belt (Sage, 2000; Stott et al., 2002; Fig. 1). An apparently similar occurrence has also been reported from the Slave Craton (Armstrong and Barnett, 2003) but is not considered here. Sage (2000) interpreted the Sandor dike as spessartite, an amphibole-rich example of Rock's (1984) calc-alkaline or shoshonitic lamprophyre clan. These rocks are termed shoshonitic lamprophyres in this paper, based on their Archean association with other shoshonitic rock types and for simplicity.

Diamonds from the MGB localities are clear, mainly white to yellow (Fig. 2) and were extracted by non-contaminating caustic fusion techniques from a suite of mutually crosscutting dykes, diatremes, and other fragmental rocks (Stott et al., 2002). Tens of thousands of microdiamonds and hundreds of macrodiamonds have been recovered in the MGB and the largest in situ diamond reported to date is 0.9 cts (Schiller, 2003). Stachel et al. (2004) report significant differences in the properties of diamonds from two Wawa breccia occurrences. Differences include diamond form, which varies from dominantly 0.3 to 1.7 mm cubes at one occurrence to 0.5 to 3.0 mm octahedra and strongly resorbed dodecahedra at the second locality. Diamond N content is highly variable at both of these occurrences, spanning a range from <10 to 600 ppm.

Several diamonds fragments were identified in samples of lamprophyre dike in Lorrain Township in the western Abitibi belt and subsequently four macrodiamonds and 95 microdiamonds were recovered from 4.6 m of core that sampled a nearby lamprophyric breccia (Cabo Mining Corporation News Release, 2002). The Lorrain diamonds are divided approximately evenly into white and yellow examples. Secondary electron (SE) micrographs of MGB diamonds typically show smooth and clear surfaces. Larger examples include multiply twinned diamonds with preserved, non-resorbed, octahedral faces. In contrast, many of the Lorrain Township macro and microdiamonds exhibit resorption features such as pitted and fluted surfaces, but they appear unaffected by subsequent deformation (Fig. 2).

The Michipicoten greenstone belt and the western Abitibi greenstone belt both contain sequences of volcanism consisting of combinations of komatiitic, tholeiitic and calc−alkaline rock types. In the case of the MGB, three volcanic assemblages were defined by Williams et al. (1991). They are the Hawk, Wawa and Catfish assemblages and they correspond to volcanic cycles 1, 2 and 3 described by Sage (1994), and have approximate ages of 2900, 2750, and 2700 Ma (Sage, 1994). Seven volcanic assemblages in the Abitibi greenstone belt record semi-continuous volcanism spanning 2750 to 2697 Ma (Ayer et al., 2002). Granitic intrusions accompanied each sequence of volcanism, although a main phase of TTG granite emplacement post-dates the deposition of most supracrustal rocks (Feng and Kerrich, 1992; Corfu, 1993; Sage, 1994). The southern Superior Province is notable for the occurrence of adakite-like felsic rocks that are commonly attributed to slab melting in Phanerozoic terranes. A recent re-evaluation by Smithies (2000) argues that adakite-like rocks are not common in Archean greenstone belts older than 2.75 Ga and notes that most examples have been described from the southern Superior Province. Rather than reflecting hot subduction zones or hot subducted slab, many Phanerozoic adakites appear related to flat subduction of relatively buoyant crust (Gutscher et al., 2000). If so, then the sporadic distribution of adakitic rocks in late Archean terranes may also be related to shallow subduction instead of a distinctly higher geothermal gradient (Wyman et al., 2002).

Regional thrusting in Abitibi and Wawa greenstone assemblages was followed by localised crustal extension

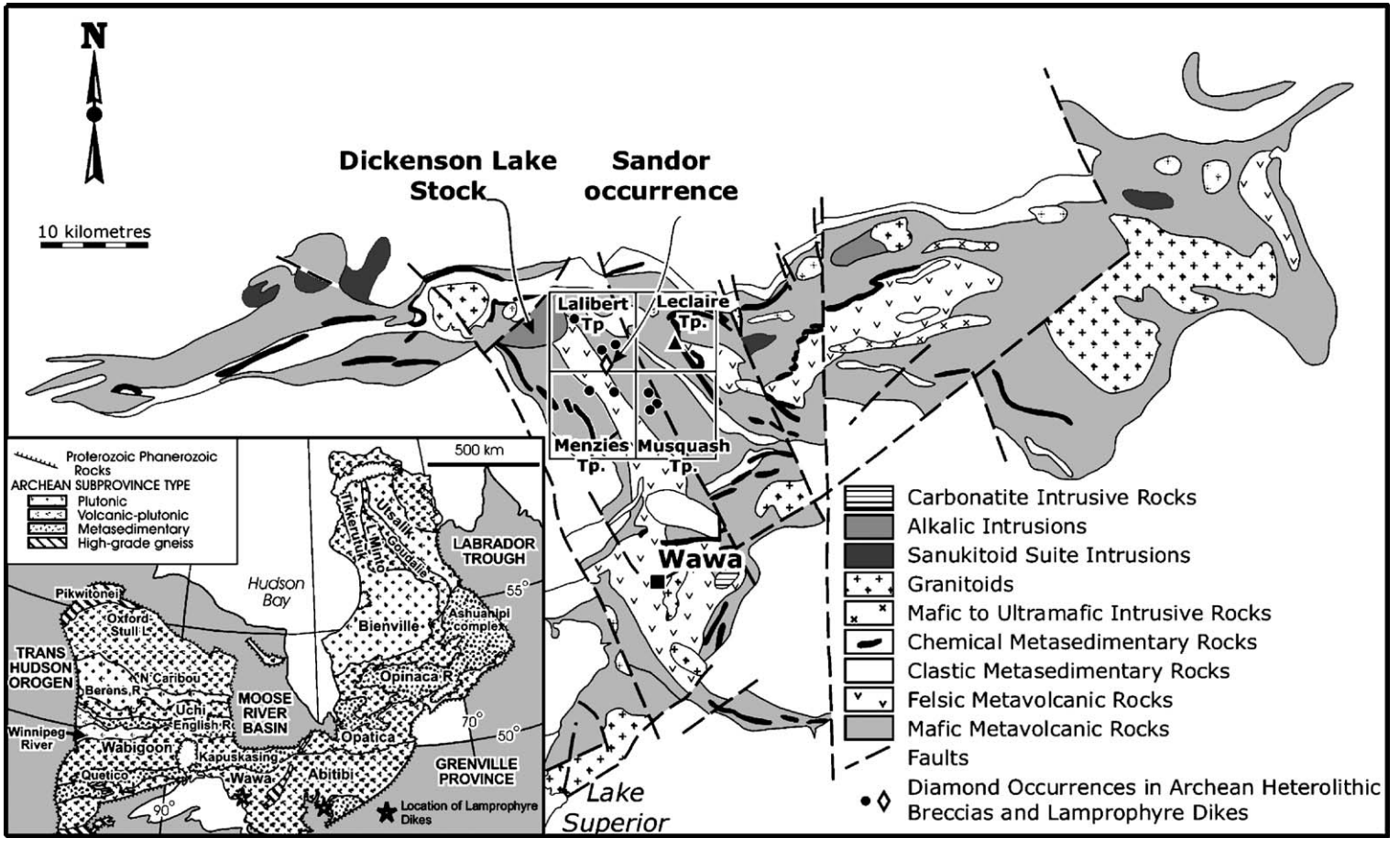

Fig. 1. Simplified map showing the localities of diamond-bearing lamprophyre occurrences in the Michipicoten greenstone belt (MGB). Inset: General locations (stars) of diamond-bearing lamprophyres in the Michipicoten greenstone belt in the Wawa Subprovince and the Cobalt area–Lorrain Township locality in the Abitibi Subprovince.

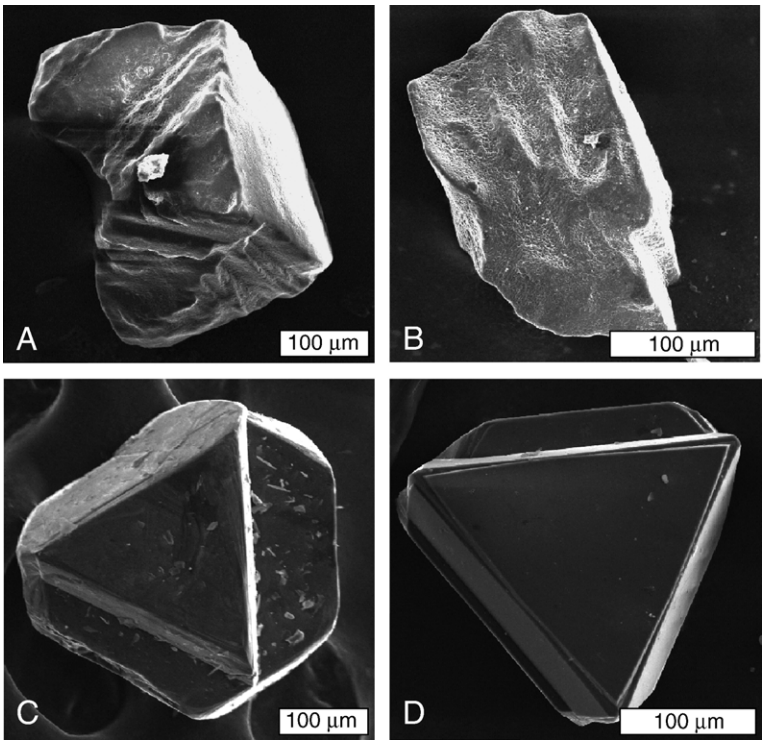

Fig. 2. Secondary electron (SE) micrographs of diamonds from Lorrain Twp showing pumice-like surface texture (A and B) and from Wawa (C and D) with flat uneroded surfaces and sharp apices. Diamond in Figure C processed by disk mill, magnetic separation and heavy liquid separation. Diamond in Figures A, B, and D processed by caustic dissolution. All SE micrographs collected on a JEOL 6400 scanning electron microscope (SEM) using a beam current 0.07 nA. Figures A and B collected using 10 keV accelerating voltage (due to excessive charging), Figures C and D collected using 20 keV accelerating voltage.

between 2680 and 2670 Ma (Ayer et al., 2002). The late- to post-kinematic emplacement of lamprophyres, syenites and associated alkalic rock types in these greenstone belts, and across the Superior Province, indicates that the suite was commonly related to cratonisation (Wyman and Kerrich, 1989, 1993). Late Archean minettes, spessartites, and other shoshonitic lamprophyres are now recognised on several cratons and commonly display a preferred association with major structures (Wyman and Kerrich, 1988; Perring et al., 1989). In the Superior Province they are generally among the youngest members of the moderately alkalic shoshonitic suite in any given area. Petrographic and mineralogical features, such as complex zoning in clinopyroxenes and high-Ti cores in micas (5–10 wt.% TiO_2), indicate crustal-level crystal fractionation commonly occurred in conjunction with magma mixing and (or) mass transfer during auto-metasomatic processes (Wyman and Kerrich, 1993).

A wide variety of geodynamic models have been applied to the Superior Province in order to account for features such as magnesian komatiites that are typically considered to have a mantle plume origin. Nonetheless, there is a strong consensus that horizontal tectonics were required to produce the calc-alkaline volcanic suites that are intermingled with komatiites-bearing sequences. Some form of plate tectonics was also required to generate many large-scale structural features, such as regional strike-slip faults (e.g., Bleeker, 2002). Evidence for a form of plate tectonics in the Superior Province includes diachronous regional deformation episodes indicative of sub-horizontal forces that added terranes to the margin of a northern cratonic core (Percival et al., 1994). Deep seismic profiles appear to reveal north vergent remnants of subducted slabs preserved in the upper mantle beneath the northern Abitibi belt and other greenstone terranes (Calvert and Ludden, 1999; White et al., 2003). The recognition of diamond-bearing magmas, derived from the mantle during the late Archean orogeny, provides an opportunity to assess these geodynamic events from an entirely new perspective.

3. Analytical techniques

The presence of diamonds in MGB and Lorrain dikes and breccias was established during commercial

exploration that employed non-contaminating caustic fusion analysis on appropriately prepared samples. To our knowledge, these studies have not established that a particular xenolith subtype is the carrier of the diamonds. Our own field studies of the host rocks were followed by petrographic and chemical analysis of representative lithological varieties such as dikes and heterolithic breccias and carefully separated examples of xenoliths and matrix material. Comparable studies of apparently barren Archean lamprophyres were undertaken in other localities in the Wawa and Abitibi Subprovinces. The results for these localities and previously published lamprophyre data (Wyman and Kerrich, 1989, 1993) provided a basis for comparisons with the diamondiferous occurrences. Small near circular mafic-ultramafic intrusions are common in the MGB and therefore represent a potential shallow-crustal source of xenoliths (Sage, 1994). Relatively fresh material from one example, the Deep Lake intrusion, was sampled via diamond drill core in order to assess this possibility.

Major element concentrations were determined using XRF and trace elements were determined by inductively coupled mass spectrometry (ICP-MS) using the facilities and methods of the Ontario Geological Survey's Geoscience Laboratories (Tomlinson et al., 1998). The U–Pb age determinations on spatially-related rocks were carried out that the Jack Satterly Geochronology Laboratory at the University of Toronto.

Isotopic analyses for Sm–Nd, and Pb–Pb were undertaken on a sub-set of samples at the geological isotope facilities of the Universidade Federal do Rio Grande do Sul (Porto Alegre, Brasil). Approximately 0.5 to 0.8 g of each sample was crushed in an agate mortar and leached with HCl 0.1 N in order to eliminate the crustal alteration. Then, the leached residue was digested with HF, HNO_3, HCl, and a solution was prepared in HCl 2.5 N. For isotopic analyses, an aliquot of the HCl 2.5 N solution was spiked with ^{149}Sm–^{150}Nd tracers in Teflon vials and warmed for one week on a hot plate until complete mixing had occurred. Column procedures used cationic AG-50W-X8 (200–400 mesh) resin in order to separate REE, followed by Sm and Nd separation using anionic LN-B50-A (100–200 μm) resin. Each sample was dried to a solid and then loaded with 0.25 N H_3PO_4 (Sm and Nd), on appropriate filaments (single Ta for Sm, and triple Ta–Re–Ta for Nd). The samples were run in a multi-collector VG Sector 54 thermal ionisation mass spectrometer at Laboratório de Geologia Isotópica (Universidade Federal do Rio Grande do Sul, Brazil) in static mode. Nd ratios were normalized to $^{146}Nd/^{144}Nd = 0.7219$. Measurements for La Jolla gave $^{143}Nd/^{144}Nd = 0.511859 \pm 0.000010$. Blanks were <150 pg for Sm, and <500 pg for Nd.

4. Field characteristics and petrography

The host rocks include 3 to 4 m wide dikes, that usually crosscut volcanic stratigraphy at high angle and heterolithic breccias up to 70 m across (Fig. 3). Stratigraphic relationships between regional volcanic

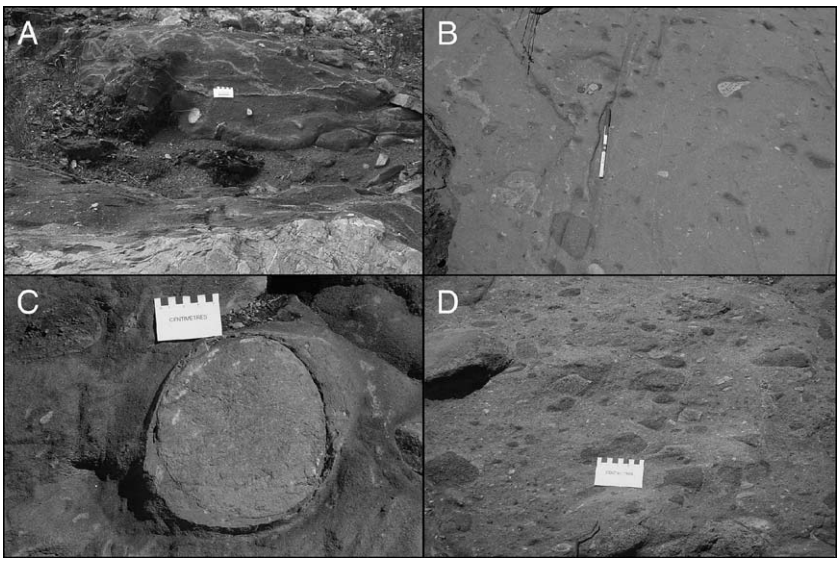

Fig. 3. Field occurrences of diamondiferous Archean lamprophyres. A. Lorrain: early lamprophyre phase with heterolihic xenoliths and flow laminations along contacts. B. Heterolithic xenoliths in MGB lamprophyre. C. Large rounded talcous ultramafic xenoliths in MGB lamprophyre dike, D. MGB lamprophyre dike with syenitic, hornblende gabbro fragments, and other inclusions.

units and the breccias are difficult to resolve in some instances. Lefebvre et al. (2003) interpreted the breccias as extrusive and therefore placed them in the upper part of the Catfish volcanic assemblage (ca. 2700 Ma), which would imply a significant gap between the breccias and dikes (ca. 2680 Ma). However, Stott et al. (2002) observed heterolithic breccia that appears to transect the surrounding MGB volcanic rocks, including dacitic lapilli tuff and pillowed basalt. A foliation that is oriented parallel to dike walls in the MGB dikes is interpreted as preferred planar alignment of minerals developed during emplacement. This foliation is overprinted at an oblique angle by a regional flattening foliation that affects the surrounding metavolcanic rocks (Stott et al., 2002).

The breccias and the inclusion-bearing dikes each appear to represent several episodes of intrusive activity resulting in a) crosscutting dikes; b) dikes that appear to be slightly younger than, but almost coeval with, the breccias; c) breccias containing fragments of inclusion-bearing lamprophyre; and d) dikes having complex intrusive relationships with syenite dikes near the Dickenson Lake syenite stock (Sage, 2000; Stott et al., 2002). It is notable that diamond has also been recovered from dikes and heterolithic breccia at the Abitibi Lorrain Township locality. The occurrence of dikes and breccias at both localities argues against an accidental association and strongly supports a genetic and temporal link between the two lamprophyric facies. Moreover, the presence of relatively large breccia bodies at both localities distinguishes them from typical late Archean lamprophyre occurrences in the Superior Province (Wyman and Kerrich, 1989).

The diamond-associated dikes are also distinguished from typical Archaean lamprophyres by the presence of abundant rounded to sub-angular ultramafic xenoliths up to 1 m in diameter (Sage, 2000). The xenoliths weather in positive relief and are altered to fine-grained assemblage of actinolite, talc, and carbonate that display a dark micaceous outer envelope, probably reflecting a reaction rim. A small proportion of xenoliths are characterised by irregular reaction fronts between outer zones of fine-grained mica and inner amphibole-rich cores that contain course phlogopite grains up to 3 mm in width (Fig. 4). Other xenoliths include sub-angular banded-gneiss, pillow basalt fragments, granite, late syenite, and other local supracrustal lithologies. Lamprophyric clasts also occur in the Lorrain Township heterolithic breccia.

Most shoshonitic lamprophyres in the Superior Province are altered and metamorphosed to the extent that igneous mafic minerals are not preserved. Wyman and Kerrich (1993) did, however, identify Abitibi minettes with unaltered diopsidic pyroxenes that retained compositional zoning and mica phenocrysts with yellow-brown phlogopitic cores and darker brown Mg-biotite rims. Primary mafic phenocrysts are also rare in the diamondiferous samples. Dike and breccia matrices are characterized by a green to greenish-black, medium-grained, granoblastic to decussate groundmass. The breccias typically have a fine-grained foliated mafic to ultramafic matrix consisting of assemblage of actinolite with variable amounts of chlorite, albite, epidote, and titanite. Macrocrysts of aluminous amphibole (mainly magnesiohornblende) and diopside occur locally in the MGB dikes and breccias (Stone and Semenyna, 2004). Williams (2002) reports that Lorrain dikes may also contain relict primary micas with "battlement" textures that range from phlogopite to biotite, based on Mg/Fe ratios. Rare partially preserved pyroxenes in the Lorrain Township samples have diopsidic compositions. Igneous chromite occurs as an accessory but widespread spinel phase in both the MGB and Lorrain occurrences (Sage, 2000; Williams, 2002). Primary textures are often obscured by the development of a post-emplacement fabric. In the case of the mica-rich Lorrain dike, however, distinct rounded aggregates of amphibole, with or without chlorite and carbonate, are common (Fig. 4A, B; Williams, 2002). The aggregates lack the fine-grained amphibole rims that are characteristic of ultra-mafic xenoliths. Similar "pilite" aggregates are common in shoshonitic lamprophyres and generally represent an alteration product of olivine (Velde, 1968; Rock, 1984). Locally, the amphibole aggregates dominate the rock and are surrounded by mica-rich domains that define a net-like texture (Fig. 4). The petrographic evidence strongly suggests that the pilite aggregates pseudomorph cumulate olivine that was surrounded by intercumulate micaceous magma. Williams (2002) also reports the presence of rounded calcite ± feldspar ± chlorite ± biotite segregations in dikes of the Cobalt area around Lorrain Township. These features correspond to the "globular structures" described by Rock (1984) as common in shoshonitic lamprophyres. Relict chromites are generally characterised by high Zn contents, typically 2.5 wt. % but as high as 4 wt.%, at both the MGB and Abitibi localities (Table 1). Similar chromite compositions are reported for diamond-bearing Archean lamprophyres from the Slave Craton (Armstrong and Barnett, 2003). These compositions may not be particularly diagnostic, however, given that Williams (2002) also reports similar compositions from apparently non-diamondiferous Abitibi lamprophyres from several localities.

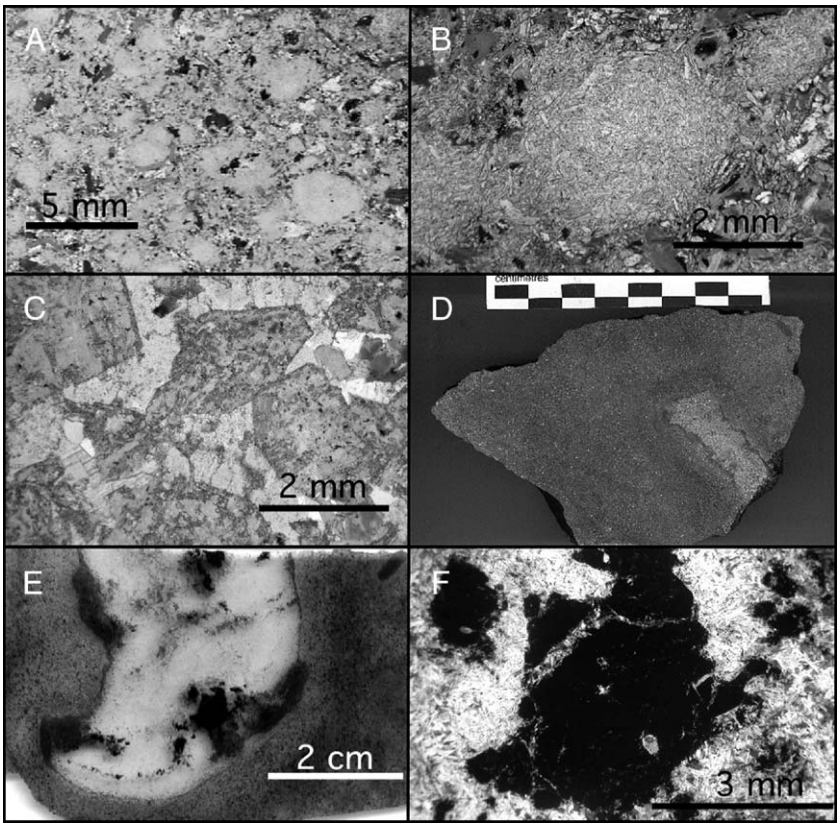

Fig. 4. A. Aggregates of "pilite", pseudomorphs after olivine crystals, in a micaceous matrix. Lorrain lamprophyre. Flatbed scan, unpolarised light. B. Close up of pilite pseudomorph, plane-polarised light. C. Relict amphibole phenocrysts in a Cobalt area dike. D. Irregularly-shaped xenolith with reaction rim in MGB lamprophyre (Sandor locality). E. Irregular xenolith of D with phlogopite masses. Flatbed scan, unpolarised light. F. Close up of phlogopite mass in E. Plane polarised light.

Low-Zn chromites also occur in the dikes (Table 1) but may be derived from ultramafic xenocrysts. For example, ophiolitic chromites from ultramafic cumulates and chromitite layers have ZnO contents as low as 0.03 wt.% (Liipo et al., 1995).

In summary, the dikes and breccias exhibit many characteristics that are typical of the calc-alkaline or shoshonitic lamprophyres. Field relations demonstrate a late-tectonic time of emplacement for the diamond host rocks that is analogous to non-diamond bearing minettes (mica–K-feldspar), spessartites (amphibole–plagioclase) and other lamprophyres in the Superior Province. The most distinctive features in outcrop are the prevalence of ultramafic clasts and the prominence of breccia facies, although these are not entirely unique across the Superior Province. Although the pilite olivine pseudomorphs observed in the Lorrain dike are common in shoshonitic lamprophyres, the high concentration of these features in the diamond-hosting intrusion is not typical of Archean lamprophyres of the Province or younger counterparts.

5. Results

5.1. Major and compatible trace element data

New analyses of lamprophyres, heterolithic breccias, ultramafic inclusions and samples of dike and breccia matrix were analysed for major and trace elements and representative analyses are given in Tables 2 and 3. The sample sets include the MGB dikes and breccias, Lorrain Township dikes and breccia, dikes from localities near Lorrain Township collectively referred to here as Cobalt dikes, as well as Abitibi localities not known to be associated with diamonds. The Cobalt dikes are chemically distinct from the Lorrain lamprophyres but share many characteristics with MGB dikes and breccias. To date, however, no diamonds have been reported from areas represented by the Cobalt samples. Previously published major and trace element data for Archean lamprophyres of the Wawa and Abitibi Subprovinces are included in chemical plots for comparison purposes (Wyman and Kerrich, 1989, 1993).

Table 1
Chromite analysis for Wawa (MGB) Lamprophyre—Sandor locality

Sample chromite	SiO_2	TiO_2	Nb_2O_5	Al_2O_3	Cr_2O_3	V_2O_5	MgO	CaO	MnO	FeO	NiO	ZnO	Total	Fe_2O_3	FeO	Total
BAG1-1	0.04	0.24	0.00	7.54	51.51	0.29	0.31	0.00	1.68	35.09	0.10	2.62	99.42	6.48	29.26	100.07
BAG1-3	0.01	0.31	0.00	13.59	53.21	0.05	6.69	0.01	0.36	23.76	0.10	0.10	98.19	0.59	23.23	98.25
BAG4-1	0.02	0.00	0.00	21.67	38.73	0.15	1.90	0.02	1.32	33.56	0.11	2.20	99.68	4.69	29.34	100.14
BAG4-2	0.13	0.13	0.00	17.17	39.35	0.13	0.90	0.00	1.53	37.60	0.17	2.41	99.53	8.47	29.98	100.37
BAG4-3	0.10	0.11	0.02	17.58	43.52	0.11	1.13	0.00	1.48	32.34	0.12	2.14	98.65	3.03	29.61	98.96
BAG4-4	0.50	0.15	0.07	12.39	39.63	0.30	0.76	0.01	1.66	40.65	0.15	2.24	98.51	11.81	30.03	99.70
BAG4-5	0.09	0.01	0.00	15.12	48.41	0.16	0.75	0.00	1.63	30.78	0.01	2.53	99.49	1.34	29.58	99.62
BAG4-6	0.06	0.01	0.00	5.93	53.60	0.07	0.36	0.01	1.82	35.09	0.13	2.23	99.30	7.28	28.54	100.03
BAG4-7	0.12	0.35	0.02	4.19	56.49	0.34	0.16	0.00	1.84	33.20	0.00	2.51	99.21	4.46	29.19	99.66
BAG5-1	0.11	0.06	0.00	20.86	40.18	0.23	0.80	0.00	1.41	32.25	0.10	4.15	100.15	3.09	29.47	100.46
BAG5-2	0.04	0.00	0.05	13.44	50.12	0.07	1.91	0.01	1.42	30.73	0.11	1.94	99.82	2.87	28.14	100.11
BAG5-3	0.02	0.00	0.01	13.44	51.05	0.09	3.30	0.00	1.33	30.27	0.03	0.58	100.12	3.05	27.53	100.42
BAG5-4	0.01	0.03	0.01	11.18	53.59	0.15	1.04	0.00	1.54	30.81	0.12	1.46	99.96	1.41	29.55	100.10
BAG5-5	0.25	0.04	0.00	4.49	61.03	0.15	0.43	0.00	1.66	29.23	0.06	2.30	99.64	0.49	28.79	99.68
BAG5-6	0.05	0.17	0.00	6.15	53.98	0.30	0.36	0.02	1.72	34.07	0.00	2.45	99.27	5.58	29.05	99.83
BAG5-7	0.08	0.00	0.01	13.39	49.06	0.19	0.59	0.00	1.56	31.21	0.03	3.59	99.71	2.73	28.76	99.98
BAG5-8	0.27	0.00	0.01	4.68	60.62	0.21	0.42	0.01	1.78	29.22	0.12	2.52	99.85	0.68	28.61	99.92
BAG5-9	0.03	0.00	0.01	13.29	49.01	0.21	0.54	0.00	1.49	31.44	0.05	3.62	99.68	2.93	28.80	99.97
BAG5-10	0.32	0.00	0.00	4.89	60.56	0.16	0.30	0.00	1.78	28.87	0.00	2.88	99.75	0.35	28.55	99.78
BAG5-11	0.08	0.07	0.00	4.43	60.74	0.08	0.32	0.02	1.79	30.01	0.00	2.71	100.23	1.80	28.38	100.41
BAG5-12	0.12	0.17	0.00	4.58	57.17	0.24	0.26	0.01	1.88	32.87	0.00	2.60	99.90	4.48	28.84	100.35
BAG5-13	0.25	0.00	0.00	4.72	60.76	0.24	0.33	0.00	1.69	29.45	0.10	2.55	100.09	0.59	28.92	100.15
BAG5-14	0.07	0.03	0.02	12.15	51.33	0.18	0.53	0.00	1.58	31.15	0.04	2.31	99.39	1.63	29.69	99.55
BAG5-15	0.08	0.16	0.05	5.03	58.71	0.09	0.38	0.01	1.78	31.86	0.09	2.47	100.70	3.33	28.86	101.03
BAG5-16	0.04	0.10	0.00	13.64	49.10	0.06	0.64	0.01	1.45	30.96	0.09	3.47	99.56	2.56	28.66	99.82
BAG5-17	0.04	0.02	0.04	12.83	49.90	0.13	0.51	0.00	1.63	30.88	0.06	3.36	99.40	2.41	28.71	99.65

The MGB and Lorrain dike and breccia samples, including separated matrix, have silica contents between 46 and 54 wt.%. Five MGB dike matrix samples have MgO contents between 10 and 21 wt.% but three MGB breccia matrix samples display a more restricted range of 20 to 21 wt.%. Breccia and matrix samples from all localities have TiO_2 contents between 0.6 and 1.5 wt.%. By comparison, the TiO_2 content of Archean-aged lamprophyric rocks in the Superior Province is generally less than 2 wt.% and mostly less than 1.5 wt.% whereas younger non-shoshonitic lamprophyres in the Province have contents ranging between 2 and 5 wt.% (Wyman and Kerrich, 1989). The diamond-associated occurrences are characterised by low P (mainly <0.5 wt.% P_2O_5: Table 2) and Al_2O_3 contents mainly between 8 and 15 wt.% that are comparable to non-diamondiferous Archean lamprophyres (Wyman and Kerrich, 1993). These compositions are distinct from olivine lamproites which typically have $P_2O_5 > 1$ wt.%, $TiO_2 =$ 3–4 wt.%, and $Al_2O_3 \approx 4.5$ wt.% at MgO ≈ 24 wt.% and far higher concentrations of LREE (Mitchell and Bergman, 1991).

Variation diagrams in Fig. 5 illustrate that the diamond-bearing dikes and breccias tend to have higher Mg contents than typical southern Superior Province lamprophyres, although there is considerable overlap. Two types of xenoliths are discernible on the basis of Mg contents. The most frequently sampled group of ultramafic xenoliths has MgO contents between 20–24 wt.% whereas two samples have MgO ≈ 30 wt.%. If one high-Al xenolith ($Al_2O_3 = 7.8$ versus 1.2–2.5 wt.%) is removed from the main group then the remaining 11 samples exhibit a restricted range of abundances for many elements (e.g., $SiO_2 = 55.3$–57.5 wt.%; $Fe_2O_3 =$ 6–8 wt.%; Ni = 1200–1400 ppm). Based on the variation diagrams for SiO_2, Al_2O_3, TiO_2, or Ni, the xenoliths cannot be mixed with typical Superior Province lamprophyres to generate the high-Mg diamond related rock types. Samples of the Deep Lake mafic–ultramafic intrusion are compositionally distinct from the xenoliths. Although the Deep Lake samples lie along extensions of lamprophyre chemical trends for many elements, a well-defined sub-trend for MGB dikes and breccias on a plot of Ni versus MgO does not extrapolate to these samples. Major element trends defined by the high-Mg samples on these variation diagrams extend toward the composition of olivine. The Ni contents of lamprophyre olivines are highly

Table 2

A. Major and trace element abundances for Wawa subprovince samples

Sample series	97RPS	97RPS	96RPS	96RPS	96RPS	GG	GG	GG	GG	GG	02DS *	02DS	02DS89	02DS	02DS90	02DS94	02DS96	MUSQ	GG	97RPS	97RPS	96RPS	96RPS	96RPS
Sample number	0004	0002	0013	0014	0012	00688	00683	00684	00689	00685	86	87	89	88	90	94	96	1	00687	0001	0003	0015	0016	0017
	Wawa (MGB) diamondiferous-matrix					Wawa (MGB) diamondiferous-whole rock					Heterolithic breccia-matrix			Heterolithic breccia-whole rock						Late lamprophyre dikes that intrude diamond-bearing lamprophyre dike set.		Deep Lake		
SiO_2	51.03	49.86	48.48	49.68	48.46	49.77	46.55	48.18	46.57	46.91	48	47	47	51	52	53	49	50.28	47.62	51.39	51.87	49.93	41.27	45.41
TiO_2	1.47	1.08	0.96	0.91	0.71	1.04	1.16	1.04	1.00	0.82	0.74	0.72	0.75	0.85	1.11	0.68	0.90	1.03	0.82	1.25	1.22	0.47	0.49	0.36
Al_2O_3	10.80	11.83	11.31	10.25	9.10	12.53	12.63	11.93	9.94	7.90	8.99	9.31	8.95	11.23	14.08	10.92	12.50	12.41	14.61	15.08	15.22	8.62	4.83	5.21
Fe_2O_3	11.30	11.04	11.44	10.41	9.80	11.10	11.86	11.41	10.99	11.08	11.03	11.01	10.77	11.13	11.73	9.03	10.75	10.73	11.45	11.42	11.18	14.21	19.26	16.61
MnO	0.15	0.17	0.18	0.16	0.14	0.14	0.16	0.16	0.14	0.17	0.17	0.17	0.17	0.18	0.19	0.13	0.16	0.14	0.17	0.23	0.17	0.17	0.25	0.17
MgO	10.17	11.59	12.35	13.99	20.49	10.68	13.18	13.20	18.39	24.32	19.75	20.36	21.56	13.18	8.90	13.47	10.28	9.52	11.50	6.86	6.82	19.99	31.36	30.07
CaO	8.69	9.21	9.32	9.22	6.59	7.11	9.37	8.94	7.07	8.02	10.06	10.19	9.73	8.79	6.27	6.98	8.44	8.36	9.74	8.00	8.61	3.88	2.43	2.14
K_2O	4.34	2.99	3.84	2.91	4.08	3.04	2.89	2.65	4.81	0.19	0.27	0.23	0.21	1.21	1.23	1.59	4.37	4.90	1.60	3.84	4.08	2.08	0.07	0.02
Na_2O	1.52	2.00	1.77	2.11	0.35	4.22	1.87	2.23	0.56	0.30	1.09	0.92	0.32	2.49	4.23	3.48	2.79	2.32	2.25	1.58	0.50	0.64		
P_2O_5	0.53	0.22	0.35	0.35	0.29	0.38	0.34	0.26	0.51	0.30	0.33	0.33	0.32	0.23	0.13	0.24	0.37	0.32	0.24	0.37	0.32	0.01	0.04	
Cr	560	612	689	740	1130	504					1358	1426	1438	792	503	873	602	398		202	212	1376	2508	2175
Co	45	49	49	48	59	44	54	53	61	74	79	80	79	68	66	56	61	49	48	38	37	97	156	125
Ni	283	365	388	487	805	310	383	404	593	954	830	840	821	435	263	504	336	239	337	118	126	1117	1579	1538
Rb	151	99	149	94	130	108	66	60	150	5	9	7	3	32	34	54	183	206	46	130	122	63	2	1
Sr	821	937	448	1013	153	324	520	492	112	119	162	176	86	373	413	552	519	483	440	701	860	35	84	47
Cs	3.55	2.37	5.95	5.22	5.97	6.63	1.91	1.77	6.89	0.34	1.22	1.06	0.35	3.06	3.62	2.90		10.21	1.99	3.24	3.63	2.47	0.18	0.05
Ba	988	947	801	1240	551	470	836	747	1269	35	66	32	266	689	508	405	2054	755	513	918	545	375	40	35
Sc	23.7	24.4	26.9	23.7	19.6	26.3	29.4	29.3	26.8	25.6	22.1	22.2	21.0	29.0	34.9	18.3	26.7	33.0	30.6	23.3	24.3	13.6	9.4	11.3
V	195	205	208	190	168	213	203	209	218	165	168	163	146	200	258	131	200	207	208	190	191	109	104	108
Ta	0.36	0.25	0.22	0.27	0.12											0.35		0.12		0.78	0.32	0.26	0.18	0.11
Nb	8.1	5.3	4.2	5.3	1.6	4.1	3.7	3.6	3.5	1.2	4.2	4.4	4.2	3.4	4.0	5.0	4.3	4.0	3.0	10.7	6.2	3.3	3.1	1.4
Zr	148	122	91	112	99	98	59	67	96	45	69	69	91	82	88	115	95	87	30	145	145	68	62	37
Hf	3.3	2.2	1.9	2.8	2.4	2.8	1.7	1.8	2.7	1.2	2.0	1.9	2.4	2.2	2.3	2.8	2.4	2.3	0.9	2.7	2.6	1.8	1.3	0.8
Th	3.5	2.7	2.5	3.7	2.7	2.2	2.1	2.5	3.0	1.9	1.9	1.8	3.2	1.7	1.4	3.5	3.7	1.6	1.8	5.7	5.5	3.4	1.9	1.2
U	1.0	0.6	0.6	0.8	0.6	0.8	0.6	0.7	0.8	0.4	0.5	0.4	0.4	0.4	0.3	0.9	1.1	0.5	0.5	1.5	1.1	1.0	0.5	0.3
Y	22.7	21.4	20.7	17.5	17.5	19.5	19.3	16.9	17.4	14.7	15.8	15.3	14.3	19.6	23.1	16.3	19.4	17.3	16.6	26.4	24.3	13.6	11.8	5.4
La	27.7	22.4	17.7	28.9	17.0	19.0	15.9	16.2	16.2	12.4	16.2	15.3	15.2	13.8	10.1	23.8	20.6	15.2	11.8	44.1	49.8	10.0	6.7	4.7
Ce	67.9	52.8	40.6	65.7	38.1	44.4	35.0	34.8	42.1	29.1	35.5	34.4	35.5	30.3	23.0	50.5	44.4	35.4	26.0	104.7	116.2	20.5	13.3	9.5
Pr	9.3	7.2	5.7	9.1	5.2	6.3	5.5	5.1	5.5	4.3	4.7	4.5	4.7	4.1	3.1	6.4	5.8	4.8	3.7	13.4	14.5	2.5	1.6	1.2
Nd	42.0	31.3	24.8	37.4	22.0	26.9	25.1	22.2	24.5	18.7	20.1	18.8	19.4	17.8	14.5	25.5	24.9	21.1	16.0	54.7	58.6	9.4	6.4	4.7
Sm	9.1	6.5	5.5	7.6	5.0	6.1	5.6	5.0	5.7	4.2	4.0	4.1	4.3	4.0	3.5	4.7	5.7	4.4	3.4	9.3	9.7	1.9	1.4	1.0
Eu	2.3	1.7	1.7	2.2	1.5	2.2	1.7	1.6	1.6	1.1	1.2	1.2	1.3	1.4	1.3	1.4	1.8	1.4	1.2	2.3	2.3	0.5	0.4	0.3
Gd	6.7	4.9	5.0	6.4	4.5	5.2	5.2	4.5	5.0	3.8	3.5	3.4	3.6	3.9	3.8	3.9	5.0	4.2	3.4	6.1	6.1	1.9	1.3	0.9
Tb	0.8	0.6	0.7	0.8	0.6	0.7	0.7	0.6	0.7	0.5	0.5	0.5	0.5	0.6	0.7	0.5	0.6	0.6	0.5	0.8	0.8	0.3	0.2	0.1
Dy	4.5	3.7	3.7	3.8	3.1	3.7	3.7	3.2	3.4	2.9	2.9	2.7	2.7	3.4	4.0	2.9	3.5	3.2	3.1	5.0	4.6	1.6	1.0	0.7
Ho	0.8	0.7	0.7	0.7	0.6	0.7	0.8	0.7	0.7	0.6	0.6	0.6	0.5	0.7	0.9	0.6	0.7	0.6	0.7	0.9	0.8	0.3	0.2	0.1
Er	2.1	1.9	2.0	1.8	1.5	1.9	1.9	1.6	1.8	1.5	1.6	1.6	1.4	2.0	2.6	1.6	1.9	1.8	1.7	2.5	2.3	0.9	0.5	0.4
Tm	0.3	0.3	0.3	0.2	0.2						0.2	0.2	0.2	0.3	0.4	0.2	0.3	0.2		0.4	0.3	0.1	0.1	0.0
Yb	1.7	1.6	1.7	1.6	1.3	1.7	1.7	1.5	1.6	1.4	1.5	1.4	1.3	2.0	2.5	1.5	1.8	1.5	1.6	2.3	2.0	0.9	0.6	0.4
Lu	0.2	0.2	0.2	0.2	0.2	0.3	0.2	0.2	0.2	0.2	0.2	0.2	0.2	0.3	0.4	0.2	0.3		0.2	0.3	0.3	0.1	0.1	0.1
Cu	64	17	47	49	13						595		26	68	77	13	46	193		46	53	234	223	43
Zn	124	113	101	104	91	92	106	102	111	84	104	108	111	103	90	84	111	94	94	112	136	108	120	116
Ag	3.09	3.05	4.14	3.09	2.06															3.04	3.04	3.13	2.36	2.27
Pb	8.24	12.20				4.94	6.14	5.39	1.73	3.48	8.41	7.39	5.25	8.28	8.21	10.18	11.13	6.07	6.01	13.18	19.26			

(La/Yb)cn	11.68	10.01	7.34	13.17	9.03	8.13	6.59	7.75	7.24	6.35	7.81	7.83	8.30	5.02	2.92	11.38	8.34	7.45	5.20	14.04	18.06	8.19	8.68	9.04
(La/Sm)cn	1.98	2.24	2.07	2.44	2.19	2.02	1.84	2.11	1.83	1.89	2.64	2.44	2.30	2.22	1.85	3.24	2.35	2.26	2.21	3.05	3.32	3.39	3.17	3.20
(Eu/Eu*)cn	0.86	0.89	0.95	0.93	0.96	1.16	0.98	1.00	0.88	0.85	0.98	0.95	0.95	1.07	1.11	0.99	1.03	1.00	1.06	0.87	0.86	0.75	0.88	0.84

B. Major and trace element abundances for Abitibi subprovince samples

Sample series	GG	02JAA	GG	GG	GG	GG	GG	GG	GG	GG	GG	GG	GG	GG	GG	GG	GG	GG	GG	GG
Sample number	00674	0002	00673	00672	00671	01674	00680	00666	00604	00612	00601	00695	00632	00635	00633	00631	00665	00675	00636	
	Lorraine Township						Cobalt Area													
SiO_2	54.58	48.44	48.54	46.60	48.01	46.24	51.20	52.54	48.23	51.20	50.56	50.42	48.26	49.46	49.95	53.08	49.65	48.15	43.57	
TiO_2	0.60	0.99	0.74	0.85	0.63	0.60	0.84	0.84	0.99	0.60	0.81	0.81	0.82	0.74	0.70	0.64	1.46	0.61	0.47	
Al_2O_3	12.06	10.72	6.61	9.77	9.45	8.81	18.05	12.85	15.37	12.97	12.79	12.06	13.58	10.73	12.80	12.51	8.00	9.14	9.73	
Fe_2O_3	8.82	10.74	11.25	10.90	9.75	9.95	11.40	10.19	14.39	12.26	11.64	11.65	11.60	11.33	10.88	11.54	14.55	10.67	11.99	
MnO	0.13	0.19	0.30	0.29	0.24	0.24	0.16	0.18	0.54	0.15	0.23	0.21	0.17	0.21	0.17	0.14	0.29	0.16	0.45	
MgO	11.35	14.57	17.15	18.29	18.36	20.69	6.35	8.52	11.05	11.13	11.17	11.85	12.30	12.57	13.24	13.40	14.59	19.23	24.37	
CaO	5.14	8.83	12.53	7.87	8.11	9.03	8.73	8.81	4.47	10.97	8.53	8.48	8.58	10.14	8.39	6.20	8.65	7.40	8.75	
K_2O	2.69	3.19	1.19	4.14	4.04	3.70	1.10	2.91	0.87	1.01	1.04	1.62	1.82	0.60	1.62	0.65	0.90	3.06	0.16	
Na_2O	4.18	1.69	0.44	0.73	1.03	0.27	2.10	2.56	3.27	1.65	2.77	2.45	2.48	3.71	1.93	1.54	1.73	1.24	0.13	
P_2O_5	0.45	0.63	1.24	0.56	0.38	0.46	0.08	0.60	0.81	0.33	0.45	0.45	0.40	0.50	0.32	0.29	0.19	0.34	0.39	
Cr		956				>500	118	258			500		500				474			
Co	37	69	43	59	58	55	44	20	58	49	85	111	46	51	49	43	35	61	70	
Ni	276	354	236	354	527	571	93	51	141	319	184	181	226	273	286	271	317	622	700	
Rb	114	154	31	192	154	138	47	65	45	29	40	58	73	20	70	21	17	41	11	
Sr	352	893	343	447	409	316	359	401	116	330	238	210	652	369	611	255	36	200	35	
Cs	8.68	8.01	1.03	12.02	11.68	12.10	1.06	1.21	3.40	2.49	1.15	2.88	7.97	2.91	7.62	4.70	0.54	1.15	5.46	
Ba	547	1307	753	958	889	511	159	547	255	270	512	600	656	168	630	289	172	641	23	
Sc	21.1	25.6	27.7	20.0	24.7	25.0	30.1	14.3	39.2	26.9	31.0	32.2	32.7	31.8	31.8	25.4	11.8	17.6	29.5	
V	156	171	133	146	183	168	177	115	218	257	181	185	283	199	248	194	110	171	162	
Ta	0.58	0.33	0.69	0.61	0.70				0.54								0.89			
Nb	5.3	6.1	10.5	8.6	13.3	9.9	3.5	4.9	12.2	2.7	5.1	3.9	4.2	3.6	3.8	2.9	11.4	4.0	2.3	
Zr	138	182	127	128	106	128	69	143	162	74	104	83	81	89	79	70	142	81	49	
Hf	3.5	4.5	3.2	3.8	2.4	3.2	1.9	4.0	3.9	1.8	2.5	2.4	2.2	2.1	2.1	1.8	3.8	1.9	1.3	
Th	3.9	3.7	8.3	4.3	3.8	7.8	2.9	4.1	4.3	2.5	3.3	3.2	2.3	2.3	2.5	2.4	6.8	0.6	1.6	
U	1.2	1.3	0.5	0.9	1.2	1.3	0.9	1.4	1.3	0.8	1.0	1.0	0.7	0.8	0.8	0.7	2.2	1.1	0.7	
Y	21.1	23.1	49.9	25.5	24.0	21.6	16.8	25.0	43.2	19.1	27.6	19.3	24.2	24.0	22.1	16.9	27.1	12.3	16.1	
La	26.9	35.1	74.2	56.0	53.1	67.3	10.6	28.2	65.0	10.3	18.8	14.6	20.1	15.8	17.7	17.6	10.8	12.9	15.9	
Ce	56.3	80.1	183.1	123.9	112.0	152.5	20.2	65.3	134.2	21.8	35.9	32.4	42.5	30.0	36.4	33.3	33.6	27.3	23.5	
Pr	7.0	11.1	26.3	16.7	14.7	18.0	2.9	8.7	18.4	2.9	5.6	4.6	6.5	4.4	5.4	4.8	5.1	3.9	3.7	
Nd	28.8	48.0	116.4	68.5	57.9	73.0	12.1	38.0	72.5	12.1	23.8	20.3	27.0	19.1	22.0	18.8	22.8	16.5	15.1	
Sm	5.8	9.6	23.9	12.1	9.8	11.8	2.9	8.2	12.2	2.7	5.8	5.0	5.2	4.2	4.3	3.5	5.1	3.4	2.9	
Eu	1.5	3.0	5.4	3.0	2.4	2.7	0.9	2.4	3.6	1.0	1.4	1.3	1.4	1.2	1.4	0.9	1.4	1.0	0.7	
Gd	4.9	7.7	20.4	10.0	7.8	9.3	3.0	7.1	9.8	2.9	5.3	4.9	4.5	4.1	3.8	2.9	5.2	3.2	2.6	
Tb	0.7	1.0	2.6	1.2	1.0	1.1		1.0	1.3		0.8	0.7	0.6	0.6	0.6		0.8			
Dy	3.1	4.8	10.2	4.7	4.1	4.7	3.1	4.7	5.9	2.6	3.8	3.7	3.4	3.4	3.0	2.2	4.7	2.4	2.2	
Ho	0.7	0.9	1.7	0.8	0.8	0.8	0.6	0.9	1.2	0.6	0.8	0.7	0.8	0.7	0.7	0.5	1.0	0.5	0.5	
Er	1.7	2.2	3.1	1.7	1.6	1.9	1.7	2.3	2.8	1.6	2.0	1.9	2.1	2.0	1.8	1.4	2.8	1.4	1.4	
Tm		0.3	0.3					0.3	0.4								0.4			
Yb	1.5	1.8	2.1	1.5	1.5	1.7	1.6	2.3	2.5	1.7	1.9	1.9	2.0	1.8	1.8	1.4	2.6	1.2	1.3	
Lu	0.2	0.3	0.3	0.2	0.2	0.3	0.2	0.3	0.4	0.2	0.3	0.3	0.3	0.3	0.3	0.2	0.4	0.2	0.2	
Cu		45				19					10		79							
Zn	81	160	109	185	180	173	79	48	418	65	298	93	79	115	74	73	50	68	344	
Ag													3.33	2.12	2.22	2.02			2.14	
Pb	7.71	12.29	2.18	2.35	3.55	1.50	21.81	8.84	44.59	1.97	12.24	17.78	7.41	3.68	5.89	4.76	23.36	8.87	4.27	
(La/Yb)cn	12.55	14.02	25.88	27.10	25.43	27.93	4.76	8.83	18.47	4.46	7.24	5.61	7.06	6.18	7.17	8.93	2.94	7.73	9.02	
(La/Sm)cn	3.02	2.37	2.01	2.98	3.49	3.67	2.40	2.22	3.45	2.45	2.10	1.90	2.51	2.40	2.67	3.28	1.36	2.46	3.52	
(Eu/Eu*)cn	0.84	1.04	0.72	0.80	0.81	0.76	0.95	0.94	0.99	1.06	0.76	0.79	0.85	0.90	1.04	0.83	0.83	0.94	0.75	

*02DS Series samples are reproduced from Stone and Semenyna (2004).

Table 3
Major and trace element abundances for xenoliths in Wawa subprovince lamprophyres

Sample series	Websteritic ultramafic xenoliths											Non-websteritic ultramafic xenoliths			Gneissic xenolith
Sample number	96-RPS	97RPS	97RPS	96-RPS	97RPS	97RPS	97RPS	97RPS	97RPS	97RPS	02JAA	02JAA	96-RPS	96-RPS	02JAA
	0011	0008	0009	0010	0006	0007	0005	0010	0012	0011	0014	0013	0008	0009	0012
SiO_2	55.29	55.52	56.01	57.37	57.50	56.04	56.16	56.18	57.13	56.14	55.75	48.08	60.93	56.72	52.54
TiO_2	0.03	0.04	0.03	0.09	0.03	0.04	0.03	0.06	0.03	0.05	0.09	0.26	0.05	0.04	0.84
Al_2O_3	1.90	1.93	2.00	1.76	1.44	2.48	1.23	2.13	1.65	2.31	1.76	7.77	2.34	3.37	16.64
Fe_2O_3	1.55	1.45	1.42	0.99	1.15	1.33	1.10	1.81	1.66	1.92	2.44	4.07	0.70	0.60	4.50
FeO	5.58	5.08	4.84	4.19	3.81	4.8	3.61	5.12	4.53	4.91	4.08	9.59	4.52	4.91	6.72
MnO	0.28	0.24	0.21	0.16	0.17	0.17	0.19	0.21	0.22	0.21	0.13	0.22	0.05	0.13	0.09
MgO	19.78	20.99	21.39	22.42	23.86	23.08	23.43	20.74	21.44	20.88	23.04	20.62	29.62	30.03	6.83
CaO	14.51	13.77	13.24	12.20	11.28	11.25	13.46	12.76	12.44	12.66	12.41	8.65	0.67	2.98	2.90
Na_2O	0.19	0.14	0.14	0.08	0.07	0.05	0.08	0.23	0.20	0.25	0.14	0.10	N.D.	N.D.	5.71
K_2O	0.03	0.04	0.03	0.10	0.04	0.08	0.05	0.07	0.04	0.04	0.56	1.61	0.19	0.03	3.79
P_2O_5	N.D.	N.D.	N.D.	N.D.	N.D.	N.D.	N.D.	N.D.	N.D.	N.D.	N.D.	N.D.	N.D.	N.D.	0.12
Cr	1703	1750	1536	1430	1439	1874	1473	1299	1438	1380	1590	3981	1349	1822	207
Co	45	56	53	57	56	61	58	53	57	58	64	85	76	71	79
Ni	1293	1399	1376	1353	1212	1294	1304	1224	1264	1266	1279	1063	1691	1787	131
Rb	0.1	0.5	0.2	3.0	1.0	2.5	1.2	0.9	0.3	0.3	21.1	67.5	5.5	1.1	160.9
Sr	94	105	99	109	128	91	291	80	74	79	102	22	57	253	294
Cs	0.02	0.05	0.05	0.38	0.10	0.28	0.17	0.04	0.04	0.03	1.60	3.21	0.37	0.12	7.80
Ba	21	N.D.	N.D.	27	23	77	46	54	17	8	259	346	23	N.D.	819
Sc	3.10	3.08	3.07	3.08	3.13	4.10	3.16	3.05	2.04	2.04	4.09	18.65	N.D.	1.10	31.45
V	90	85	88	59	50	60	46	105	85	107	34	123	37	41	212
Ta	0.03	N.D.	N.D.	0.03	N.D.	N.D.	N.D.	N.D.	N.D.	N.D.	N.D.	N.D.	0.04	0.03	N.D.
Nb	0.12	0.05	0.04	0.17	0.05	0.08	0.08	0.03	0.03	0.03	0.45	0.34	0.15	0.12	3.04
Zr	9.31	10.27	10.25	10.28	10.42	10.25	13.69	10.15	9.17	10.19	N.D.	N.D.	9.57	8.79	53.14
Hf	0.04	0.07	0.05	0.06	0.06	0.05	0.05	0.06	0.02	0.04	N.D.	0.12	0.09	0.03	1.49
Th	0.02	N.D.	N.D.	0.07	0.04	0.05	0.04	N.D.	N.D.	N.D.	0.06	N.D.	0.20	0.41	N.D.
U	N.D.	N.D.	N.D.	0.08	0.08	0.34	0.06	N.D.	0.07	0.09	0.08	0.03	0.02	0.04	0.10
Y	1.36		2.21	1.32		2.27	1.88		1.68	3.16	1.53	1.91	0.55	1.31	13.15
La	0.13	0.28	0.19	1.60	1.75	1.45	5.14	7.01	8.85	26.76	4.08	0.33	1.17	7.06	3.18
Ce	0.26	0.45	0.49	2.40	2.58	2.18	7.91	13.57	16.88	51.84	5.54	0.69	3.07	16.74	8.90
Pr	0.05	0.08	0.10	0.34	0.36	0.36	0.97	1.75	2.20	6.62	0.67	0.13	0.47	2.35	1.49
Nd	0.41	0.65	0.68	1.63	1.94	1.53	4.35	8.07	9.64	29.09	2.88	0.71	2.22	9.61	7.82
Sm	0.14	0.27	0.23	0.36	0.43	0.36	0.68	1.08	1.18	3.58	0.43	0.25	0.44	1.63	2.48
Eu	0.05	0.26	0.38	0.20	0.30	0.16	0.28	0.59	0.45	1.01	0.16	0.10	0.11	0.45	1.00
Gd	0.19	0.30	0.26	0.32	0.40	0.29	0.44	0.58	0.46	1.28	0.42	0.36	0.27	0.88	2.81
Tb	0.02	0.06	0.04	0.04	0.04	0.04	0.05	0.07	0.05	0.11	0.05	0.05	0.02	0.09	0.43
Dy	0.17	0.35	0.24	0.22	0.25	0.23	0.31	0.47	0.29	0.68	0.28	0.30	0.12	0.25	2.56
Ho	0.03	0.08	0.05	0.03	0.04	0.04	0.05	0.08	0.04	0.09	0.04	0.06	0.01	0.03	0.53
Er	0.10	0.26	0.18	0.11	0.13	0.12	0.17	0.26	0.16	0.33	0.12	0.20	0.04	0.12	1.45
Tm	0.01	0.04	0.03	0.01	0.02	0.02	0.02	0.04	0.02	0.04	0.02	0.03	N.D.	0.01	0.20
Yb	0.13	0.31	0.28	0.12	0.13	0.13	0.17	0.26	0.14	0.28	0.12	0.20	0.05	0.13	1.17
Lu	0.02	0.06	0.05	0.02	0.02	0.02	0.02	0.05	0.02	0.04	0.02	0.03	0.01	0.02	0.17
Cu	N.D.	N.D.	N.D.	N.D.	7.30	16.40	15.79	6.09	N.D.	6.11	43.98	N.D.	N.D.	N.D.	204.93
Zn	95.21	73.95	60.46	58.60	66.71	76.87	72.64	80.22	93.71	92.74	107.38	130.52	93.60	92.34	83.19
Ag	1.03	2.05	2.05	N.D.	1.04	1.02	1.05	2.03	2.04	2.04	N.D.	N.D.	N.D.	N.D.	N.D.
Pb	N.D.	N.D.	N.D.	8.22	8.34	18.45	17.90	13.20	8.15	36.69	16.36	7.25	N.D.	N.D.	9.13
(La/Yb)cn	0.72	0.65	0.50	9.32	10.04	7.78	21.87	19.03	44.51	69.73	23.84	1.21	15.77	38.36	1.95
(La/Sm)cn	0.60	0.67	0.56	2.88	2.65	2.60	4.85	4.21	4.84	4.83	6.14	0.86	1.73	2.80	0.83
(Eu/Eu*)cn	0.96	2.77	4.81	1.73	2.21	1.51	1.48	2.06	1.55	1.17	1.16	1.05	0.89	1.04	1.16
Normative minerals															
Quartz	3.73	3.52	4.28	5.86	5.57	3.95	2.68	5.25	6.35	5.23	2.05		10.88	2.33	
Plagioclase	5.88	5.77	5.95	4.85	4.12	6.76	3.55	6.55	5.25	7.23	3.68	16.71	3.32	9.16	40.80
Normative minerals															

Table 3 (*continued*)

Sample series	Websteritic ultramafic xenoliths											Non-websteritic ultramafic xenoliths			Gneissic xenolith
Sample number	96-RPS	97RPS	97RPS	96-RPS	97RPS	97RPS	97RPS	97RPS	97RPS	97RPS	02JAA	02JAA	96-RPS	96-RPS	02JAA
	0011	0008	0009	0010	0006	0007	0005	0010	0012	0011	0014	0013	0008	0009	0012
Orthoclase	0.18	0.24	0.18	0.59	0.24	0.47	0.3	0.41	0.24	0.24	3.31	9.40	1.12	0.18	22.22
Corundum													0.93		
Diopside	54.06	50.84	48.42	44.67	41.47	39.29	50.52	46.69	46.25	45.85	46.25	21.27		4.51	4.00
Hypersthene	33.76	37.38	38.99	42.37	46.81	47.47	41.21	38.29	39.41	38.52	41.02	24.80	82.55	82.78	
Olivine												21.50			16.12
Ilmenite	0.06	0.08	0.06	0.17	0.06	0.08	0.06	0.11	0.06	0.09	0.17	0.49	0.09	0.08	1.58
Magnetite	2.33	2.19	2.12	1.49	1.74	1.97	1.68	2.68	2.46	2.83	3.52	5.84	1.09	0.97	6.48
Apatite															0.28

variable and often exhibit marked zonation. For example minettes from Mascota, Mexico, have NiO contents of 0.57 wt.% in their cores and rims with NiO contents as low as 0.15 wt.% (4480 to 1180 ppm Ni; Carmichael et al., 1996). The trend to high MgO contents defined by the Archean lamprophyres can be accounted for by addition of olivine with average Ni contents of 2000 ppm. Therefore, all of the trends in Fig. 5 could be approximated by the variable accumulation or entrainment of olivine, assuming that it contained inclusions of chromite.

5.2. Incompatible trace element data

Select trace elements are plotted on Zr variation diagrams in Fig. 6. The diamond-associated samples again display only partial overlap with the field defined by typical Wawa and Abitibi lamprophyres. Many of the samples plot at Zr values of less than 100 ppm, unlike most Superior Province lamprophyres. Some distinctions are evident between the MGB and Lorrain samples. The MGB dikes and most MGB breccia samples define a clear positive trend for Nb at Zr<125 ppm but Lorrain Township samples display no correlation between Nb and Zr correlation and lie in a distinct field, mainly at higher Zr contents (106–182 ppm). Cobalt samples overlap the MGB trend or plot with the Lorrain samples, supporting the inference that they are not typical (i.e., non-diamondiferous) Abitibi lamprophyres, which encompass a far greater range of Zr abundances.

There are broad positive correlations between Zr and other high field strength elements (HFSE) such as Nb, U, or Th for all lamprophyres in the data set at Zr contents less than ~240 ppm. The Lorrain samples alone, however, do not display strong trends. None of the lamprophyres exhibit strong correlations between the Large Ion Lithophile elements (LILE) such as Rb, or Sr and Ba (not shown) and Zr, probably because of alteration effects. Fractionation between the Heavy Rare Earths (HREE) displays a correlation with Zr for diamond-associated MGB dikes and breccias but not for the Lorrain samples. Light REE fractionation displays no correlation with Zr abundance for any of the groups.

Compositional variations among the diamond-related samples are readily distinguished on multi-element normalised plots as shown in Fig. 7. Primitive mantle-normalised plots for Lorrain Township and Cobalt district lamprophyric rocks (Fig. 7A) indicate that the Lorrain samples have higher abundances of the more incompatible elements (LREE–MREE; Th, Nb, Zr, Hf) than most Cobalt district samples. Although diamonds have not been recovered from dikes of the Cobalt area, their LREE contents and overall incompatible element abundances are similar to MGB diamond-associated dikes and breccias. Potassium is generally strongly enriched relative to the LREE in the Cobalt samples. Similar K enrichments also occur in some non-diamondiferous Abitibi lamprophyres, which display relatively uniform K contents but highly variable incompatible trace element abundances (not shown).

A multi-element plot of diamond-bearing MGB lamprophyre dikes and matrix indicates generally higher incompatible element abundances in matrix samples relative to whole rock samples (Fig. 7B). In contrast to the dikes, MGB breccia matrix samples have lower HREE contents than corresponding whole rock samples but overlapping LREE contents (Fig. 7C). Data for a small lamprophyric breccia body (MgO~7 wt.%) from the Hemlo greenstone belt approximately 150 km

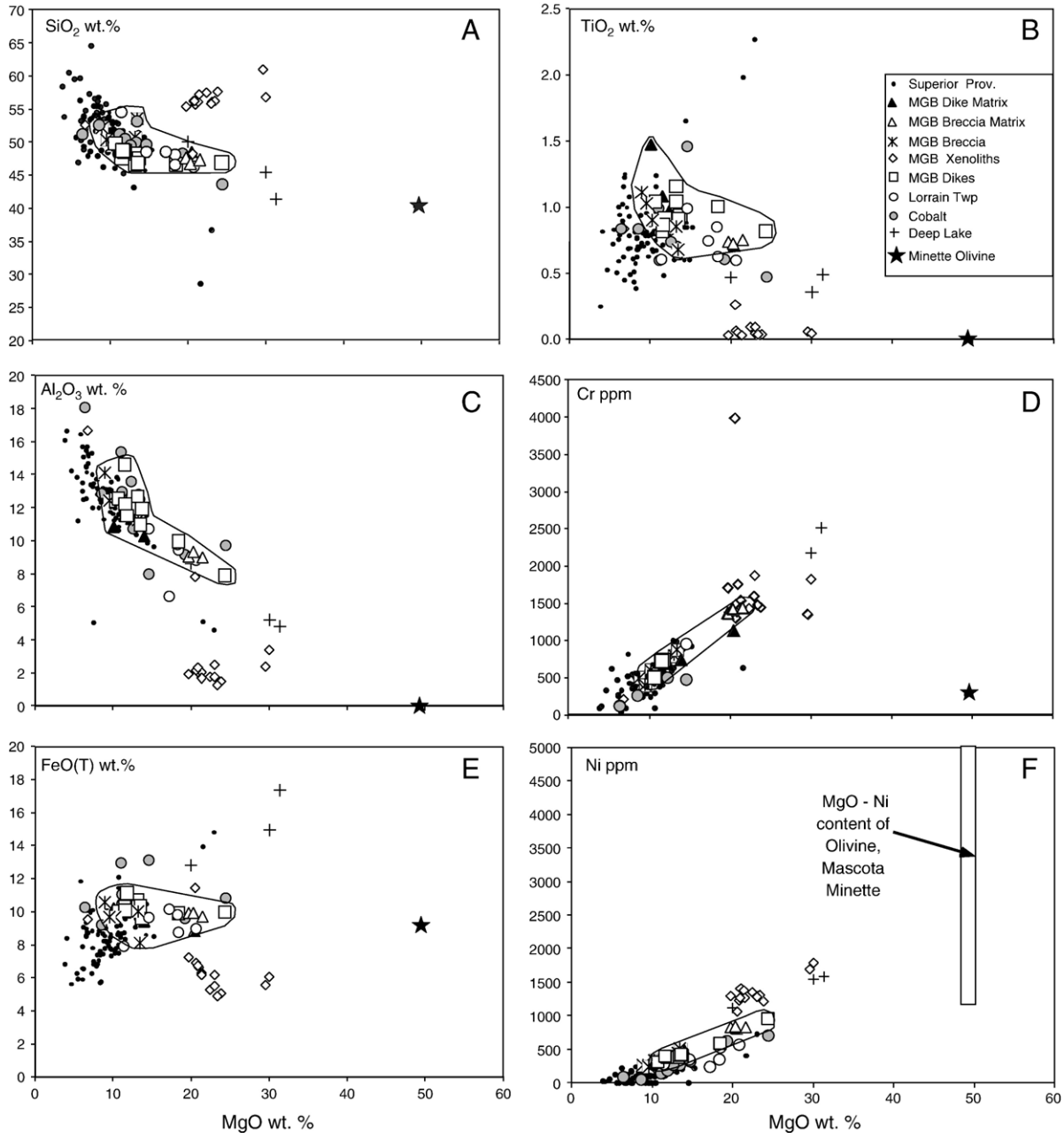

Fig. 5. Magnesium variation diagrams for major elements and compatible trace elements. Superior Province samples are non-diamondiferous lamprophyres of Wyman and Kerrich (1989, 1993). MGB = Michipicoten greenstone belt (Wawa Subprovince) samples. The MGB whole rock and matrix samples (dikes and breccia) are shown enclosed within a solid black line for ease of reference. Lorrain (township) = Abitibi Subprovince diamondiferous samples. Cobalt = Abitibi samples in the vicinity of diamondiferous lamprophyres. Deep Lake = Small mafic-ultramafic intrusion in the vicinity of MGB dikes. Minette olivine composition from Carmichael et al. (1996).

northwest of the MGB occurrences is also plotted on Fig. 7C. The comparison demonstrates that some previously recognised lamprophyres have trace element abundances directly comparable to the diamond-associated MGB dikes and breccia (Wyman and Kerrich, 1989). Muir (1997) notes that Archean lamprophyric dikes and breccias, with or without mafic/ultramafic xenoliths, are common in the Hemlo area. Archean lamprophyre dikes from the more northerly Pickle Lake greenstone belt in Uchi Subprovince (MgO ~ 12 wt.%) also have incompatible trace element contents that overlap the MGB dike and

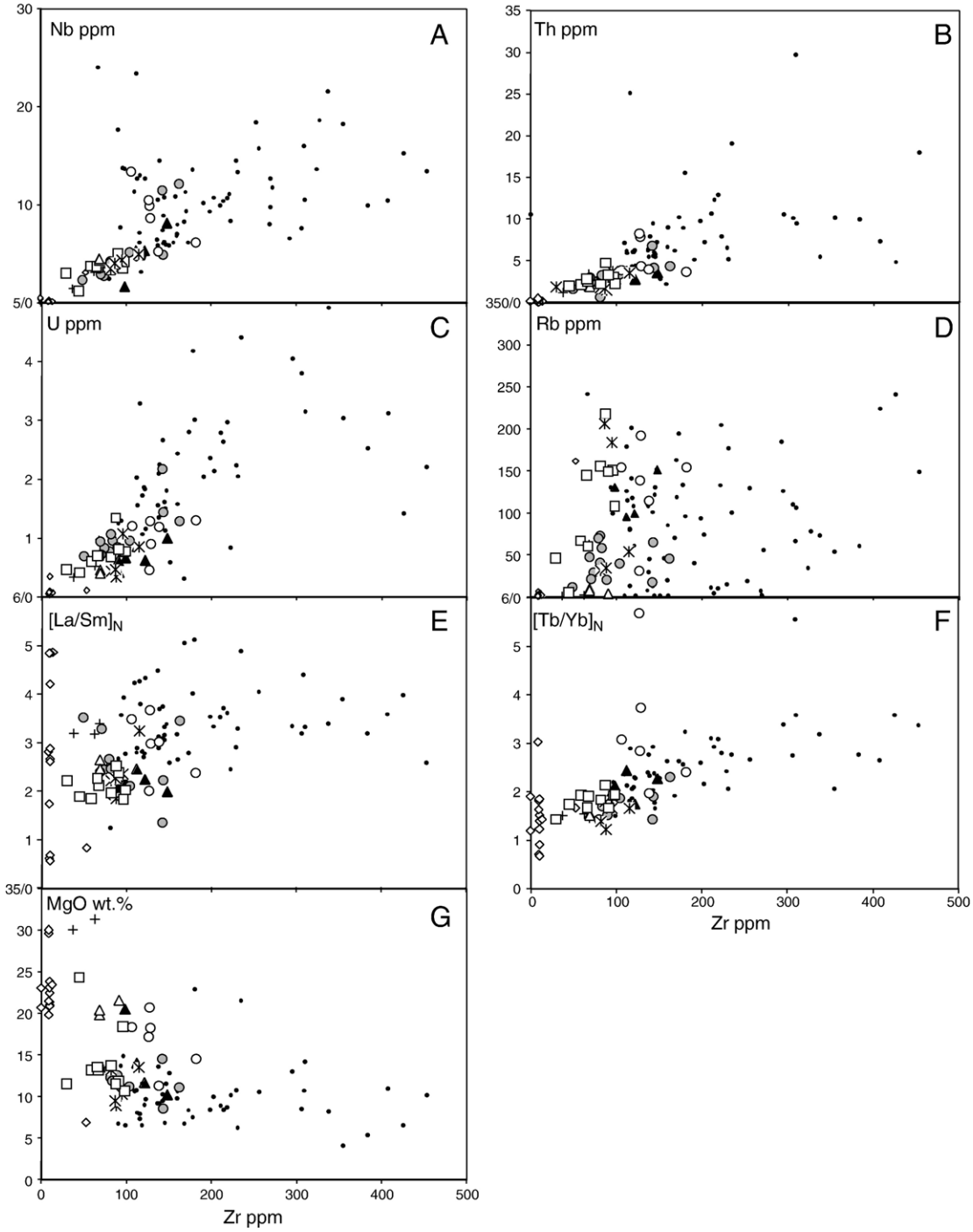

Fig. 6. Zirconium variation diagram for incompatible trace elements and MgO. Symbols as in Fig. 5.

breccia matrix compositional range (not shown; Wyman and Kerrich, 1989).

Multi-element plots for xenoliths contained within MGB dikes and three samples of the Deep Lake Intrusion are presented in Fig. 8. Despite the uniformity of major element compositions among the main group of xenoliths, there is a wide variation in their REE contents. All of the xenoliths display normalised Nb depletions and some degree of Zr–Hf depletion versus the MREE. Samples of the ultramafic Deep Lake

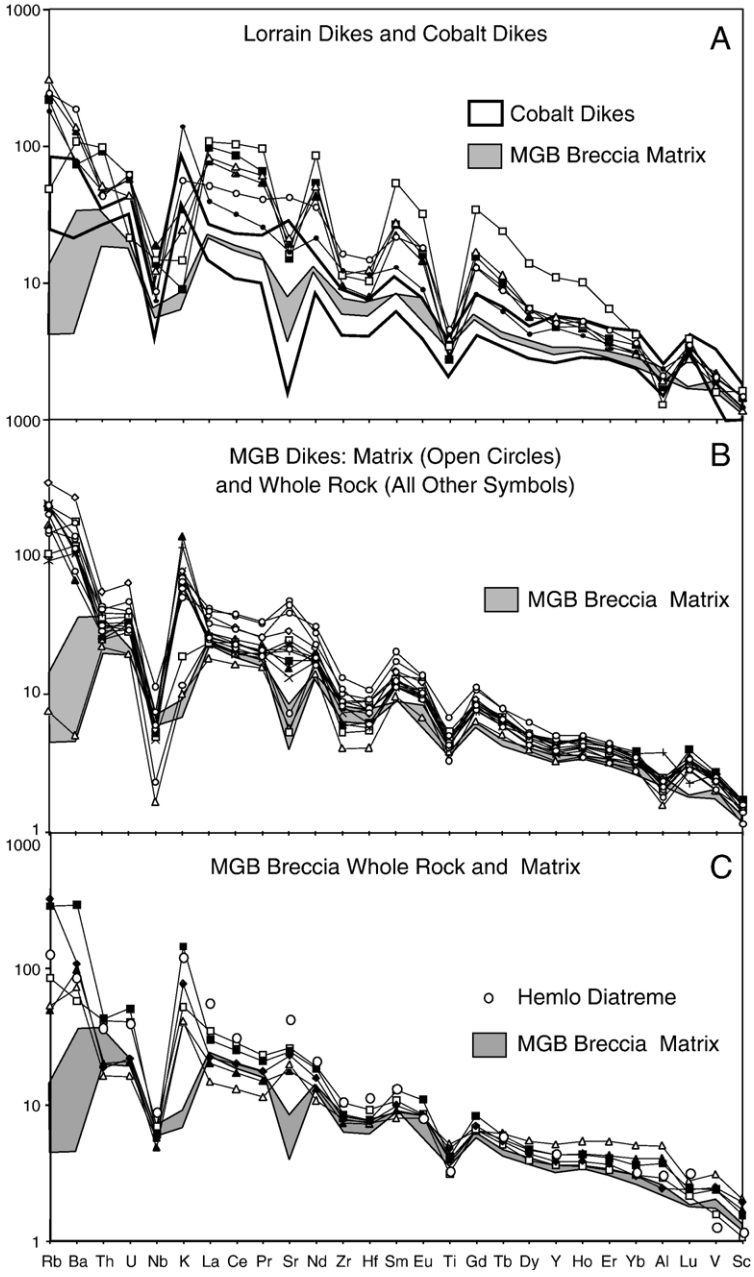

Fig. 7. Primitive mantle-normalised multi-element plots for diamondiferous lamprophyre dikes and breccias. Normalising factors after McDonough and Sun (1995). For clarity, only Lorrain samples are plotted individually in part A; the compositional range of Cobalt samples is shown as a field enclosed by thick black lines. The compositional range of MGB breccia matrix samples is included in all three panels for comparison purposes. The symbols used to distinguish individual samples in this figure do not correspond to those used to identify sample groups in previous figures.

intrusion are distinct from the xenoliths, ruling out this and similar shallow crustal bodies as the source of the xenoliths. A sample of banded gneiss xenolith displays a relatively unfractionated pattern but does exhibit strong Rb enrichment and a moderate positive Sr anomaly.

5.3. Geochronological studies

U–Pb zircon geochronological work has been ongoing to help better understand the nature and timing of the diamondiferous units and their host rocks (Vaillancourt et al., 2005). $^{207}Pb/^{206}Pb$ results to date

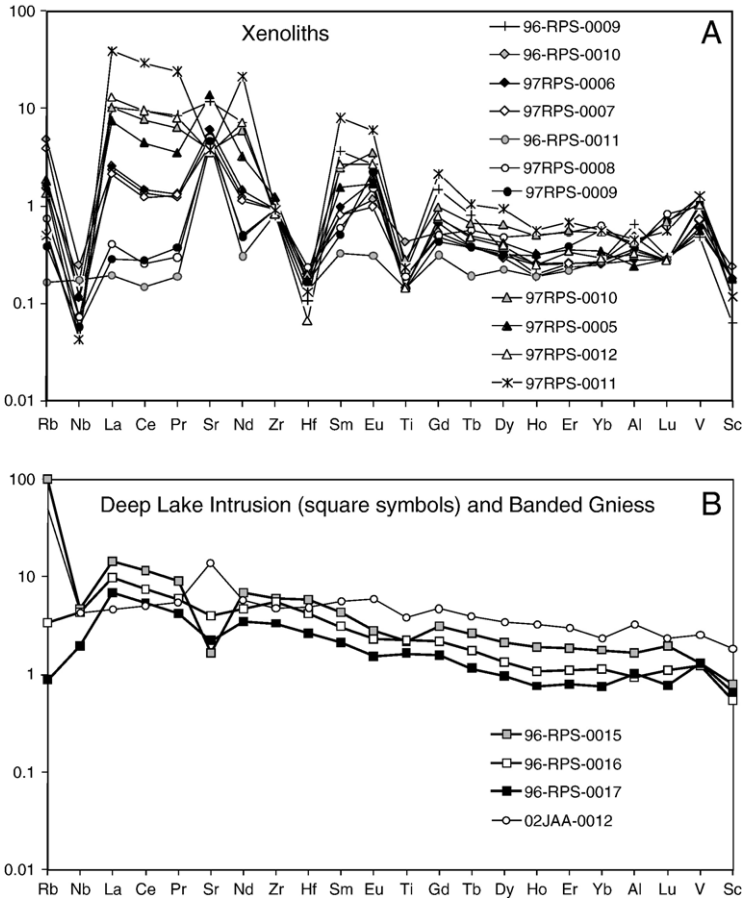

Fig. 8. Primitive mantle-normalised multi-element plots for xenoliths in diamondiferous lamprophyre dikes and breccias. All samples except 96-RPS-0009 belong to the websteritic group discussed in the text (see also, Table 3). Normalising factors after McDonough and Sun (1995).

include an age of 2701.4±2.1 Ma from a felsic volcanic unit hosting diamondiferous units and maximum ages of 2685.0±1.0 and 2684.9±1.4 Ma for diamondiferous lamprophyre dikes cutting the Catfish assemblage felsic to intermediate volcanic units in Lalibert and Menzies townships (Fig. 1). A second sample of felsic lapilli tuff adjacent to the Moet occurrence in northeastern Menzies Township contains zircons indicating a Catfish assemblage age of 2698.7±1.1 Ma (Vaillancourt et al., 2004).

Lamprophrye dikes cut the diamondiferous breccias and thus are at least slightly younger than the breccias. In order to test the age of brecciation, a sample of diamondiferous breccia from the Moet showing was collected for geochronology. Five zircons were analyzed and concordant data was obtained for each of them. The three oldest ages are 2687±2, 2683±2 and 2681±2 Ma. The two youngest zircons from this sample give data that precisely overlap each other at 2679.2±2.1 Ma (Vaillancourt et al., 2004). This is the youngest zircon age obtained from the breccia and therefore represents either the time of crystallization/emplacement of the body, providing the zircons are magmatic, or a maximum time of emplacement if the zircons are xenocrystic. In the latter case, this age must still be close to the time of breccia emplacement given that a lamprophyre dike in Musquash Township has an emplacement age of 2674±8 Ma U-Pb age, based on a titanite analysis (Stott et al., 2002).

The data indicates that felsic volcanic units hosting the diamondiferous rocks are part of the Catfish assemblage. The maximum age for the diamondiferous breccias and the associated dikes is well established at less than 2680 Ma. Collectively, these absolute age constraints indicate that the breccias are not volcaniclastic (cf. Lefebvre et al., 2003), but are related to a volatile-rich diatreme brecciation event in which mantle-derived diamonds were transported into the upper crust. These lamprophyre and breccia ages are broadly similar to an age of 2673±8 Ma obtained for the

nearby Dickenson Lake Syenite stock by Turek et al. (1992) and an age of 2674±2 Ma obtained from titanite in a non-diamondiferous minette lamprophyre of the Abitibi belt by Wyman and Kerrich (1993).

5.4. Whole rock radiogenic isotope compositions

The Sm–Nd and U–Pb isotopic compositions of a representative sub-set of MGB and Lorrain samples were determined for this study. The samples include diamond bearing and non-diamond bearing (or diamond absent) lamprophyres, ultramafic xenoliths and a sample of the Catfish Assemblage felsic volcanic rocks (Table 4). Given the extreme rarity of well-preserved primary minerals such as pyroxenes, only whole rock analyses were attempted. The volcanic sample is characterised by an εNd_T value of 2.1, which is similar to the value inferred to characterise the dominant Late Archean upper mantle source for the southern Superior Province (Shirey and Hanson, 1986; Machado et al., 1986). An Abitibi (Lorrain) lamprophyre is characterised by an εNd_T of 2.2, which is similar to, but slightly more positive than, values reported by Wyman and Kerrich (1993) for non-diamondiferous Abitibi examples (εNd_T=0.5 to 1.9 for 12 whole rock and mineral separates). The MGB lamprophyres display a relatively wide range of compositions from εNd_T=0.0 to 4.8 calculated with T=2674 Ma. It is not clear what the absolute age of the xenoliths are, although age data from zircons provides no direct evidence of Hawk assemblage volcanic ages (i.e., 2900 Ma) material in these rocks. When assigned the same 2674 Ma age used for the dikes the ultramafic xenoliths define εNd_T between 2.9 and 8.2. The latter value is distinctly high compared to most published Superior Province samples.

Whole rock Pb isotopic analyses were also undertaken on MGB and Lorrain dikes, breccias, and xenoliths. Values of $^{206}Pb/^{204}Pb$ and $^{207}Pb/^{204}Pb$ are unusually high for the diamond-related lamprophyres and xenoliths compared to the southern Superior Province as a whole and the Wawa Subprovince in particular, where galena data for three massive sulphide deposits ranges between $^{206}Pb/^{204}Pb$ of 13.15 and 13.25 and $^{207}Pb/^{204}Pb$ of 14.36 and 14.42 (Thorpe, 1999).

Table 4
Sm–Nd and Pb isotopic results for diamond-bearing lamprophyres and related samples

Sample	Rock type	Sm (ppm)	Nd (ppm)	$^{147}Sm/^{144}Nd$	$^{143}Nd/^{144}Nd$	SE %	εNd (t=today)	εNd (t=2674)
96RPS0013	Wawa (MGB) lamprophyre — M*	4.25	19.44	0.132310	0.511678	0.0039	−18.7	3.5
96RPS0014	Wawa (MGB) lamprophyre — M	5.73	29.14	0.118950	0.511268	0.0012	−26.7	0.0
02JAA-0015	Wawa (MGB) lamprophyre — WR	4.57	21.27	0.129920	0.511702	0.0066	−18.3	4.8
02JAA-0002	Abitibi (Lorraine) lamprophyre WR	5.21	24.67	0.127730	0.511534	0.0016	−21.5	2.2
97RPS0007	Websteritic xenolith	0.13	0.43	0.181720	0.512702	0.0019	1.3	6.4
97RPS0008	Websteritic xenolith	0.14	0.29	0.301640	0.514705	0.0013	40.3	4.2
97RPS0010	Websteritic xenolith	0.36	1.48	0.148225	0.512199	0.0045	−8.6	8.2
02JAA-0014	Websteritic xenolith	0.20	0.91	0.132720	0.511892	0.0015	−14.6	7.5
02JAA-0013	Non-websterite ultramafic xenolith	0.13	0.44	0.180470	0.512501	0.0014	−2.7	2.9
02JAA-0012	Mafic gneiss xenolith	2.14	4.66	0.277750	0.512337	0.0024	−5.9	−34.0
97RPS0003	Late Wawa lamprophyre	7.14	41.58	0.103820	0.511163	0.0012	−28.8	3.2
02JAA-0016	Cycle 3 volcanic	3.51	20.92	0.101540	0.511068	0.0012	−30.6	2.1

Sample	Rock type	$^{206}Pb/^{204}Pb$	SE %	$^{207}Pb/^{204}Pb$	SE %	$^{208}Pb/^{204}Pb$	SE %
96RPS0013	Wawa (MGB) lamprophyre — M	17.319395	0.0201	15.314479	0.0195	36.543764	0.0186
96RPS0014	Wawa (MGB) lamprophyre — M	17.458684	0.0212	15.353392	0.0217	36.454101	0.0218
02JAA-0015	Wawa (MGB) lamprophyre — WR	16.689860	0.0227	15.112182	0.0236	34.830415	0.0235
02JAA-0002	Abitibi (Lorraine) lamprophyre WR	15.687783	0.5180	14.837198	0.6835	34.121628	0.5251
97RPS0007	Websteritic xenolith	15.381890	1.0212	15.091564	1.0221	36.168810	0.0218
97RPS0008	Websteritic xenolith	14.842949	0.1027	14.829575	0.0912	34.851817	0.1198
97RPS0010	Websteritic xenolith	14.995248	0.0097	14.967154	0.0098	35.231583	0.0105
02JAA-0014	Websteritic xenolith	20.545820	0.0199	15.919874	0.0200	41.089059	0.0200
02JAA-0013	Non-websterite ultramafic xenolith	17.976045	0.0476	15.450641	0.0343	38.952570	0.0539
02JAA-0012	Mafic gneiss xenolith	15.734687	0.9024	13.689040	1.0598	32.684448	1.8095
97RPS0003	Late Wawa lamprophyre	15.722265	0.0137	15.060582	0.0137	35.526908	0.0138
02JAA-0016	Cycle 3 volcanic	19.712766	0.0204	15.670686	0.0196	38.649365	0.0195

*M=matrix sample; WR=whole rock sample.

6. Discussion

6.1. Host rock affinities

Some of the diamond-associated dike and breccia samples have MgO contents that are considerably greater than values published for shoshonitic lamprophyres (Rock, 1991). Many others, however, lie within the 10 and 15 wt.% MgO range that characterises mafic members of well-documented lamprophyre suites. For example, Canning et al. (1996) describe Caledonian minettes of the Scottish Northern Highlands with MgO contents up to 14.8 wt.% and Morrison et al. (1987) report other examples from Argdour, Scotland with MgO contents ranging between 6.0 and 16.4 wt.%. Similarly, Navajo minettes of Four Corners region of the Colorado Plateau contain ~5 to 16 wt.% MgO (Vaniman et al., 1985; Laughlin et al., 1985).

Petrographic evidence and major element trends indicate that high MgO contents (>16 wt.%) can be accounted for by the presence of cumulate or entrained olivine in the more mafic lamprophyres. Given that post-Archean minettes magmas commonly evolve by olivine fractionation at lower crustal depths (e.g., western Mexico: Righter and Carmichael, 1996), it is probable that the olivines represent cumulates from earlier batches of lamprophyre magma or related shoshonitic magma that predate dike emplacement.

The low abundances of incompatible elements in the MGB dikes and breccias might also be partly attributable to olivine accumulation. However, shoshonitic lamprophyres display a wide range of incompatible element abundances at a given MgO abundance that depend on several factors. For example, the Lorrain dike contains 20.7 wt.% MgO but also has the highest LREE contents of any diamond-associated sample. Canning et al. (1996) show that two suites of contemporary Caledonian minette lamprophyres, both with MgO~ 6 wt.%, differ greatly in terms of their La abundances (170 versus 43 ppm) because of differing source characteristics on either side of the Great Glen Fault. In general, amphibole lamprophyres of a given igneous province have lower incompatible element contents than mica lamprophyres of the same area (Shand et al., 1994). For example, Perring et al. (1989) illustrate examples of late Archean spessartite (amphibole–plagioclase lamprophyre) from the Yilgarn craton, Australia, with classic textures and La contents that extend as low as 9 ppm in weakly altered samples. A compilation of Rock (1991) reports the average La content of 138 minettes was 86 ppm whereas the average La content of 100 spessartites was 35 ppm. On this basis, the lower incompatible trace element contents of the amphibole-rich MGB and Cobalt suites compared to the mica-rich Lorrain dike or other Abitibi minettes is consistent with shoshonitic lamprophyre suites of all ages.

Whole rock samples of the MGB dikes have immobile incompatible element contents that overlap or are lower than corresponding matrix samples (Fig. 7B). This xenolith dilution effect in the whole rock samples is superimposed on variable olivine accumulation and causes only minor shifts in compositions. For example, the Al_2O_3, FeO, and MgO contents of the matrix samples all fall within the compositional range of the whole rock samples. Abundances of immobile incompatible elements in three MGB breccia matrix samples overlap the lowermost ranges of the dike matrix samples, supporting a co-genetic relationship between the two MGB lamprophyre facies. The Cobalt dikes, which contain comparatively few xenoliths, also overlap the composition of this magma in terms of incompatible trace element contents (Fig. 7A). Therefore, a similar type of amphibole-rich lamprophyre magma is directly (MGB) or indirectly (Cobalt) associated with both diamond occurrences in the Wawa and Abitibi Subprovinces.

In contrast to the MGB dikes, the high abundance of xenoliths in the associated heterolithic breccia impacts noticeably on the compositions of whole rock samples. Compared to matrix samples, the breccia whole rock samples are characterised by systematically higher silica contents (51–53 versus 47–48 wt.%) and higher Al_2O_3 (11–14 versus 9 wt.%) but lower MgO (9–13.5 versus 20–21 wt.%). Whole rock samples with LREE contents lower than the breccia matrix have HREE contents that are greater than the matrix (Fig. 7C). These relationships indicate that breccia whole rock sample included significant amounts of evolved gneissic crustal material, which has almost unfractionated incompatible trace element abundances, and (or) other tholeiitic greenstone belt rock types (Fig. 8B).

Chemical signatures of the mica-rich Lorrain lamprophyres are distinct from the nearby Cobalt occurrences and correspond to a different but similar magma type. Few studies of post-Archean shoshonitic lamprophyres have considered the implications of differences in the trace element contents of spatially associated primitive amphibole- and mica-bearing varieties. Shand et al. (1994) suggest that minettes are derived from deeper sources than amphibole-bearing varieties and that the higher LILE, HFSE, and LREE contents of minettes reflects smaller degrees of melting of a more extensively metasomatised mantle source (cf. Table 2).

Most post-Archean shoshonite suites are related to the termination of subduction and slab breakoff (Atherton and Ghani, 2002) or other settings that involve crustal extension above subduction-modified mantle (Carmichael et al., 1996). The large breccia bodies associated with the Archean diamond occurrences suggest favourable conditions for magma ascent from the lower crust, irrespective of differences in the depths of origin for the parental magmas. These optimal conditions most plausibly correspond to particularly pronounced, but transitory, episodes of crustal extension. Rapid magma ascent evidently also promoted the entrainment of cumulate olivine from the plumbing systems used by lamprophyre magmas and the incorporation of xenoliths from the lithospheric mantle to the shallow crust. Given the rarity of such breccia bodies, and the sporadic distribution of diamonds in Superior Province lamprophyres, these conditions are likely to also be an essential requirement of diamond preservation. The presence of diamonds clearly precludes prolonged mid-crustal magma storage and fractionation histories documented for some other Archean lamprophyres (Wyman and Kerrich, 1993).

In summary, field relations, petrographic characteristics, chemical compositions, and absolute age dates demonstrate that the diamond host rocks are closely associated with, and compositionally grade into, typical Archean shoshonitic lamprophyres. The strongly magnesian compositions of some diamond-associated dikes and breccias do not signify an entirely unique origin for these occurrences. Instead, they provide an indication of transitory episodes of crustal extension that enabled primitive examples of a relatively common suite of shoshonitic magmas to locally entrain and preserve diamonds during Archean orogeny.

6.2. *P–T* conditions of magma genesis

Experimental studies confirm that shoshonitic magmas can be derived from the decompression melting of metasomatised mantle that typically contains phlogopite (Conceição and Green, 2004). Minette and spessartite lamprophyres are part of this spectrum of broadly cogenetic magmas as demonstrated by their spatial associations with hornblendic ultramafic to intermediate rocks that share chemical trends (Fowler and Henney, 1996; Carmichael et al., 1996; Feldstein and Lange, 1999). Shoshonitic magmas of all ages are characterised by enrichments of the lithophile elements K, Rb, Ba, Cs, Th, U, and light rare earths relative to the high field strength elements (HFSE). Primitive lamprophyres exhibit a combination of high incompatible element enrichments and elevated compatible element contents. These features preclude significant crustal contamination and require derivation from a depleted mantle source that is variably enriched in LILE and LREE. These signatures are readily accounted for in subduction-related models but are rarely, if ever, addressed in alternative Archean tectonic scenarios.

As argued above, the parental magmas to the diamond host rocks were most plausibly characterised by MgO contents near 16 wt.%. Most studies imply generation, or final equilibration prior to ascent, of lamprophyre magmas near pressures of 1.5 to 2.0 GPa and temperatures of ~1150–1200 °C as deduced for the pre-eruptive mantle conditions associated with the parental magmas of Pliocene Sierra Nevada minettes (MgO = 12 wt.%; Feldstein and Lange, 1999). These source *P–T* conditions are comparable to those of absorokites, syenites and other rock types associated with many lamprophyre suites (eg, Carmichael et al., 1996; Conceição and Green, 2004), although Righter and Carmichael (1996) calculated equilibration conditions in excess of 3 GPa (~100 km depth) and 1200 °C for one primitive minette of the Colima area, Mexico.

Xenoliths in Colorado Plateau lamprophyres typically conform to these *P–T* conditions but also include volatile-rich and low-temperature (~450 °C) varieties that are derived from depths of ~60 km and linked to subduction cooling of the upper mantle (Helmstaedt and Doig, 1975; Smith, 1995; Roden and Shimizu, 2000). Nonetheless, an unusually deep source is indicated for the Thumb minette of the same area (MgO 12 wt.%; Ehrenberg, 1982), based on a distinctive xenolith suite that includes garnet peridotite which equilibrated at pressures between 4.5 and 5.0 GPa (~140–160 km depths) and temperatures between 1150 and 1370 °C. (Smith et al., 1991). The *P–T* estimates associated with the Thumb minette remain unique for post-Archean shoshonitic lamprophyres but are potentially significant for the present study of diamond-hosting occurrences. Most recent research on the Colorado Plateau minettes has focussed on the xenoliths rather than the lamprophyre host rocks. These studies imply that rapid heating of upper mantle xenoliths occurred due to the infiltration of lamprophyre magma, which in turn may have been related to incursion of hot asthenosphere (Smith et al., 1991; Riter and Smith, 1996).

Rock (1991) suggested that calc-alkaline or shoshonitic lamprophyres can be divided into two types, one consisting of the Navajo minettes and a few other minette occurrences and another consisting of amphibole-rich varieties (kersantites and spessatites), mica-bearing types with plagioclase dominated groundmasses

(vogesites) and remaining minettes. The two sub-types can be partially discriminated on a plot of TiO_2/P_2O_5 versus CaO/Al_2O_3 (Rock, 1991), although the altered MGB and Lorrain township occurrences lie in the field of compositional overlap. Nonetheless, the Archean occurrences would correspond to the non-Navajo subgroup in such a classification, given the prominence of amphibole-rich varieties in the MGB and their association with a wide variety of shoshonitic rocks such as syenites and monzonites that are derived from relatively shallow mantle sources. In addition, Navajo minettes have TiO_2 contents of 1.6–2.0 wt.% at MgO contents of 8 to 11 wt.% (Rogers et al., 1982) that are distinct from the MGB and Lorrain lamprophyres which are characterised by TiO_2~0.6 to 1.0 wt.% at MgO~ 10 wt.%. Based on these considerations, the MGB and Lorrain Township dikes and breccias are most plausibly examples of lamprophyric magmas that are generated, or equilibrate, at *P–T* conditions that are far outside those associated with the traditional diamond sources from deep within the lithospheric roots of Archean cratons.

6.3. Xenolith origins and significance

In order to constrain processes in the lower crust and lithospheric mantle at the time of lamprophyre magmatism we consider the evidence provided by the xenolith suite and the isotope systematics of the xenoliths and their lamprophyre hosts.

The major element compositions of a large proportion of the mafic–ultramafic xenoliths sampled in MGB diamond host rocks define a single population, despite the fact that they do not correspond to local shallow-crustal rock types. This xenolith group is characterised by SiO_2 contents of 55 wt.%, very low Ti contents, Al_2O_3 between 1.6 and 2.5 wt.%, Fe_2O_3 between 5 and 8 wt.% and MgO between 20 and 23 wt.% and CaO between 11 and 14 wt.%. Alteration precludes rigorous application of least squares fit analysis of major element abundances to calculate primary mineral assemblages (Herrmann and Berry, 2002). Nickel contents of these xenoliths are also relatively uniform at about 1250 ppm. However, their major element compositions lie between those of ortho- and clinopyroxene, suggesting they were originally websteritic pyroxenites. The CIPW norms of the main xenolith group also define rocks that are dominated by normative Diopside and Hypersthene (Table 3).

Pyroxenites are commonly reported among lower crustal or upper mantle xenoliths where orthopyroxene may have a primary magmatic origin or occur as a metasomatic phase related to the alteration of olivine (Garrido and Bodiner, 1999; Smith et al., 1999; Brueckner et al., 2002). Igneous websterites vary greatly in their Al contents. Websterites and other pyroxenites that occur as sheets and lenses in the Beni Bousera Peridotite Massif, Morocco, typically have Al_2O_3 contents between 7 and 15 wt.%. Pearson et al. (1993) consider the Massif to represent mantle wedge that was "marbled" with slab-derived pyroxenite melts prior to exhumation. Other websterites have much lower Al-contents (1–3 wt.%) and originate as cumulates in ophiolites and magma chambers at the base of arc crust (Féménias et al., 2003; Saccani and Photiades, 2004). For example, Parlak et al. (2002) interpret this type of pyroxene cumulate from the Pozanti–Karsanti ophiolite (Turkey) as the product of crystal fractionation of primary basaltic melts at ~10 Kbar in the absence of plagioclase. The major element compositions of the main xenolith group in the MGB lamprophyres strongly resemble these post-Archean cumulate websterites but have several percent greater SiO_2 contents.

The combination of uniform major element compositions and extremely variable trace element abundances in the main, websteritic, group of MGB xenoliths suggests heterogeneous metasomatism of a relatively uniform precursor. The two high-Mg samples (MgO~30. wt.%) have silica contents equal to or greater than the main xenolith group and both have strongly fractionated REE with $[La/Yb]_N = 16$ and 38. Accordingly, the major and trace element characteristics of the two samples cannot be linked to the websteritic xenoliths by igneous fractionation but are consistent with metasomatism acting on sub-arc lithosphere. Europium anomalies in the websteritic xenoliths range from negligible to strongly positive but become progressively less pronounced as overall REE abundances and LREE enrichment increases (Table 2). There is no correlation between the size of the Eu anomalies and xenolith Al_2O_3/TiO_2 ratios and therefore a metasomatic process most likely accounts for the variation in REE content. Both negative and moderately positive Eu anomalies are observed elsewhere in upper mantle and lower crustal pyroxenes and pyroxenites and they are frequently linked to metasomatism (Mazzucchelli et al., 1992; Beccaluva et al., 2004).

If the unmetasomatised precursors to the MGB xenoliths possessed almost unfractionated REE patterns (eg., samples 97RPS-0008, and -0009) then low degrees of metasomatism were characterised by fluctuating $Eu/Eu*$ in the fluid or melt. Where metasomatism was more pronounced then overall REE abundances are higher in

the xenoliths and LREE enrichment is greater but Eu anomalies are negligible. These trends can be accounted for by the greater mobility of Eu under low oxygen fugacities compared to the other REE and therefore document varying oxygen fugacities within the mantle domains represented by the xenoliths and (or) the metasomatic fluid or melt. This type of correlation can occur in association with a pulse of oxidised fluids similar to those responsible for fO_2 values of $\Delta FMQ \approx 2$ in young Lihir xenoliths (McInnes et al., 2001). Progressively more oxidised conditions associated with higher fluid–rock ratios would be linked to higher overall REE contents but diminished Eu anomalies.

Metasomatism involving oxidised fluids is common in xenoliths from post-Archean shoshonitic lamprophyres and shoshonitic rock types found in active arcs (McInnes et al., 2001). Accordingly, the Archean xenoliths provide additional support to a model where the lamprophyres and diamonds were generated in a geodynamic setting that was analogous to modern subduction-related orogens.

The Sm–Nd isotopic results for the lamprophyres, and particularly the websteric xenoliths, exhibit distinct trends when plotted against their respective sample Nd contents (or Sm/Nd: not shown). Fig. 9A illustrates that websterite εNd_T increases with Nd until approaching an εNd_T value of ~ 8.5. This relationship requires that the fluid or melt responsible for metasomatising the websterites was derived from a depleted and isotopically evolved reservoir. Many potential counterparts of these aged and depleted reservoirs have been identified in post-Archean terranes. Pyroxenites and high-Al websterites of the Beni Bousera Massif had εNd_T ranging between −9 and +26, at their emplacement age of 21 Ma, reflecting the large range of compositions present in the mantle wedge located above subducted slabs. Contributing melt sources included diverse mixtures of altered oceanic crust and hemi-pelagic sediments (Pearson et al., 1993). Eclogitic residue left in subducted slab after melt generation can also provide the isotopically aged and refractory source required to create an εNd_T reservoir of +8.5. Extremely high

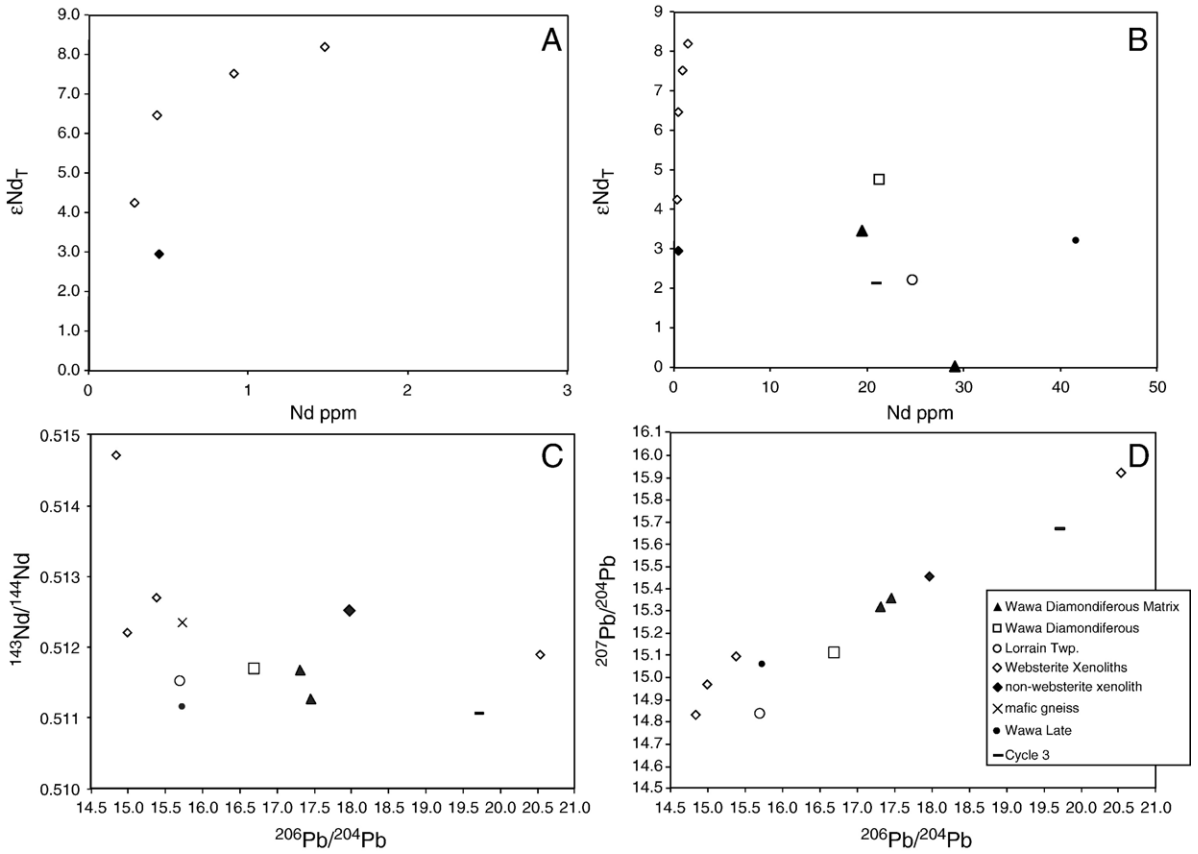

Fig. 9. Sm–Nd and Pb isotope systematics of diamondiferous Wawa and Abitibi lamprophyres and related samples (T=2674 Ma). A. εNd_T versus Nd (0–3 ppm)., B. εNd_T versus Nd (0–50 ppm)., C. $^{143}Nd/^{144}Nd$ versus $^{206}Pb/^{204}Pb$., D. $^{207}Pb/^{204}Pb$ versus $^{206}Pb/^{204}Pb$. See text for discussion.

positive values of εNd_T (up to 500) of ecologite xenoliths at the time of kimberlite emplacement attest to ancient partial melting events that were probably associated with the generation of Archean TTG (Jacob, 2004). Moreover, high εNd values also characterise strongly depleted parts of ophiolite sequences that have not been melted during subduction. Sharma et al. (1995) report present day εNd values of +9 (for gabbro) to +47 (for harzburgite) in ~400 Ma mafic and ultramafic rocks of the Voykar ophiolite, Polar Urals, which initially had an εNd of 8.6.

In the case of the Wawa Subprovince, greenstone belt volcanism and lithosphere formation extended back to at least 2.89 Ga. Accordingly, an appropriate old, low Sm/Nd, source, such as (slab) melt residue or a depleted ophiolite-style magmatic suite (Wyman et al., 1999; Coogan et al., 2003), could have acted as the source of metasomatic fluids.

Among the lamprophyres, one MGB matrix-only sample has an εNd_T of 0.0, which is distinctly low compared to most results for mantle-derived rocks analysed in the southern Superior Province. Wyman and Kerrich (1993) interpreted similar low εNd_T values and high $\delta^{18}O$ values for Abitibi lamprophyres and mineral separates as evidence for incorporation of sediments into the source regions of their parental magmas. A Lorrain diamondiferous whole rock sample has an εNd_T value of 2.2 that is slightly more positive than the 0.5 to 1.9 range reported by Wyman and Kerrich (1993). A second MGB matrix sample (εNd_T=3.5) and an MGB whole rock sample (εNd_T=4.8) are far more positive than the previously reported range.

Diamondiferous lamprophyre εNd_T increases with decreasing Nd contents so that the isotopic trend of these lamprophyres is essentially the opposite to that of the websteritic xenoliths (Fig. 9B). If this feature is related to a mixing event involving sub-arc lithosphere and lamprophyric magma then it is unlikely to have been an equilibrium AFC (assimilation–fractional crystallization) process, given that diamonds remain in the lamprophyres. Entrainment (i.e., mechanical mixing and xenolith abrasion) of deep arc crust or lithosphere during magma ascent would, however, permit diamonds to survive the mixing event. Major and trace element trends outlined above indicate that unusually Mg-rich diamondiferous lamprophyres (MgO 25–30 wt.%) cannot be generated by simple mixing of websterite xenoliths and primitive (MgO=16 wt.%) lamprophyric magma. Nonetheless, some compositional variation in the lamprophyres as a result of websterite addition is not ruled out. Websterite mixing can be assessed with reference to MGB lamprophyre matrix samples 96RPS-0013 (19.44 ppm Nd, εNd_T=3.5) and 96RPS-0014 (29.14 ppm Nd; εNd_T=0.0) and the most strongly metasomatised websterite sample 97RPS-0010 (1.48 ppm Nd; εNd_T=8.2). Simple mixing of the high-Nd matrix sample and websterite to achieve the low Nd abundance of the second matrix sample gives a "predicted" εNd_T of 3.0 rather than the measured 3.5 and requires proportions of 0.36 parts websterite to 0.64 parts magma. Discrepancies between predicted and actual major element abundance include MgO contents that are too high (16 versus 12 wt.%) and Al_2O_3 contents that are too low (7.4 versus 11.3 wt.%). The results suggest that the lamprophyre εNd_T trend is partly attributable to the incorporation of vein material with $\varepsilon Nd_T \approx 8.5$ and relatively high REE contents, along with variably metasomatised websterite xenoliths.

Analysed samples are plotted in $^{143}Nd/^{144}Nd$ versus $^{206}Pb/^{204}Pb$ space in Fig. 9C. The low REE websterite sample lies at higher $^{143}Nd/^{144}Nd$ and lower $^{206}Pb/^{204}Pb$ ratios than the depleted mantle (DM) source component of modern oceanic basalts (Hofmann, 1997 and references therein), which is consistent with its chemical makeup and long-term preservation of the xenolith. Other websterite samples document significant shifts in isotopic composition and their $^{206}Pb/^{204}Pb$ compositions bracket the range defined by lamprophyre samples. This relationship rules out the lamprophyre magmas as the main metasomatic agent acting on the xenoliths. Compared to the well-known reservoirs of modern oceanic basalts, the websterite xenolith with the highest $^{206}Pb/^{204}Pb$ value most closely resembles the HIMU mantle component (Hofmann, 1997). Its $^{143}Nd/^{144}Nd$ composition, however, appears to be intermediate between HIMU and the EMII component (Hofmann, 1997). On a plot of $^{207}Pb/^{204}Pb$ versus $^{206}Pb/^{204}Pb$ these two websterites define either end of an array that encompasses all ultramafic xenolith and lamprophyre samples (Fig. 9D). The $^{206}Pb/^{204}Pb$ composition of the late, non-diamondiferous, Wawa lamprophyre (~15.7) is distinctly lower than that of the diamond-bearing lamprophyres of the same area (≥16.69). Given that Abitibi Lorrain dike exhibits a similarly low value (15.69), it is not clear whether the isotopic distinction among the Wawa samples is particularly diagnostic.

The trace element and isotopic evidence can be accounted for in the following scenario. Low-Al websterite formed as cumulate at or near the base of the arc crust during the last major cycle of volcanism in the southern Wawa Subprovince at 2.7 Ga. The cumulate was initially characterised by εNd_T at least as low as the 4.2 value of websterite sample 97RPS0008 and possibly as low as the non-websterite sample

02JAA-0012 (εNd_T=2.9) as was typical for mantle-derived magmas at this time (Machado et al., 1986; Shirey and Hanson, 1986; Nagler and Kramers, 1998). Termination of subduction increased mantle temperatures and began to liberate fluids from the deepest parts of the orogenic complex. The sources of these fluids may have previously been subject to partial melting and hydrothermal metasomatism in order to acquire characteristics that are intermediate between HIMU- and EMII-like characteristics. These fluids metasomatised the sub-arc lithosphere, resulting in vein systems and variable εNd_T over small domains of lithospheric websterite. The refractory source of the metasomatising agent cannot have been created immediately prior to the event by TTG melt formation at 2.7 Ga. Instead, an older melting event associated with subduction or mantle plume processes created a precursor that was isolated for many 10s of million years. For example, the 5 by 25 km Hawk assemblage, located about 20 km to the SE of the MGB dikes, is dated at about 2890 Ma and contains komatiites, tholeiites, and calc-alkaline rock types (Williams et al., 1991 and references therein; Sage, 1994). Parts of this assemblage may have been underthrust during the late Archean orogeny, or may have been part of the previously cooled subduction complex that was subject to rising temperatures once subduction ceased. Either scenario can account for the presence of a suitably aged and depleted source of metasomatising fluids at ~2.67 Ga.

6.4. Diamond genesis and transport

Numerous lines of evidence indicate that diamond host rocks in the Superior Province are shoshonitic lamprophyres, which Luhr (1997) has described as the "geochemical essence of subduction zone magmatism" (p. 493). With a few exceptions, most researchers allow for the presence of some type of ~2.7 Ga subduction tectonics while not discounting that alternative tectonic processes may be required to account for specific features of individual late Archean greenstone belts or cratons (Bleeker, 2002). Mantle plume scenarios or rift tectonics without subduction cannot readily account for the major and trace element compositions of the lamprophyres, particularly since the combination of high compatible and incompatible element contents in many examples preclude extensive crustal assimilation.

The distribution of shoshonitic lamprophyres through time provides important context for the MGB and Lorrain diamond deposits. As detailed elsewhere (Wyman and Kerrich, 1988; Kerrich and Wyman, 1990), shoshonitic lamprophyres first became widespread during the late Archean where they already display a global association with quartz-carbonate vein gold deposits. This association has persisted since the late Archean and links a distinctive mantle-derived rock type with a specific style of mineralisation that is characterised by particular fluid characteristics, metal associations, structural settings, and timing relative to orogeny (McCuaig and Kerrich, 1998). The complex array of variables represented by this metallogenic association probably requires that an important thermal threshold was crossed prior to ~2700 Ma so that fluid reservoirs, orogenic P–T paths and hybridised mantle sources approximate their modern counterparts. These observations are likely to have important consequences for diamonds associated with Archean subduction.

Phanerozoic peridotite massifs and ultra-high pressure (UHP) continental crust assemblages demonstrate the return to surface of diamond formed at depths between 120 to 200 km in a subduction zone setting. The diamonds may have formed in the mantle overlying subducted oceanic crust or within the subducted assemblages themselves (Davies et al., 1993; van Roermund, 2002). Preserved examples of diamonds formed in a subduction zone setting occur in the Western Gneiss Region of Norway (Brueckner et al., 2002) and support the inferred diamond identity of graphitic pseudomorphs found elsewhere. Studies of high-pressure quartzo-feldspathic granulites, commonly containing tectonic lenses of garnet-peridotite, indicate this type of process has occurred since at least the late Archean (O'Brien and Rötzler, 2003). In principle, therefore, continentally derived UHP rock types could provide a carrier for the rapid return of MGB and Lorrain diamonds to crustal levels accessible to lamprophyre magmas. No such UHP assemblages, however, outcrop in proximity to the MGB and Lorrain lamprophyres or elsewhere in the Wawa and Abitibi subprovinces.

Whereas buoyant continental crust can be extruded up the subduction channel during active subduction (Chopin, 2003), the shallow level emplacement of peridotite massifs is generally linked to the end of subduction and orogeny (Davies et al., 1993). Although similar massifs are not present in the southern Superior Province, diamond pseudomorphs in the younger examples are noteworthy because they demonstrate that diamonds remain in the mantle wedge during orogeny. Slab detachment during the last stage of the subduction process, however, is linked to an inevitable influx of hot asthenosphere into the former mantle wedge region (Wortel and Sparkman, 2000). As noted by de Boorder et al. (1998), the hot asthenosphere incursion may represent the heat source that generates

orogenic vein gold deposits. These ore deposits mainly post-date lamprophyres in the Superior Province, although some overlap occurs. Critically, the hot, dry, asthenosphere lacks a subduction signature and cannot be a source of the lamprophyres. These factors indicate that lamprophyre generation and diamond entrainment must have been restricted to a short interval that approximately coincided with slab break off.

Diamond formation in subduction zones can occur in cold subducted slab or in the shallow mantle because the cold-finger effect of subduction creates a window into the low-*P*, low-*T* part of the diamond stability field (Barron et al., 1996; Griffin et al., 2000). In the case of the placer diamonds from SE Australia, Barron et al. (1996) invoked a stability window at about 110 km and suggested that the diamond carriers were basanite, nephelinite and leucitite magmas. Griffin et al. (2000) estimated that a low-*T* (~350 °C) source region in static subducted slab located at depths between 100 and 120 km would remain in the diamond stability field for up to a few 10s of million years following subduction.

Fig. 10 illustrates *P*–*T* conditions related to this generic Phanerozoic subduction zone diamond as modelled by Griffin et al. (2000). Application of this model to lamprophyre-related diamond deposits presents several difficulties. First, the proposed minimum depths for diamond stability are greater than those typically assigned to shoshonitic lamprophyre magmas, although they fall within the range implicated for the Thumb minette. Secondly, the dip of the slab is likely to steepen during orogeny, and carry diamonds to greater depths rather than into the zone of lamprophyre magmatism.

The minimum depth of the diamond stability field and the effect of a possibly higher Archean geotherm are illustrated using the commonly cited Archean *P*–*T* trajectory of Martin (1986) in Fig. 10B. This geotherm requires that the typical Archean graphite–diamond transition move from ~170 km to depths greater than 200 km. If all other variables are kept constant and the subduction-related perturbation of the diamond stability described by Griffin et al. (2000) is depressed 30 km deeper then its shallowest point would occur at depths

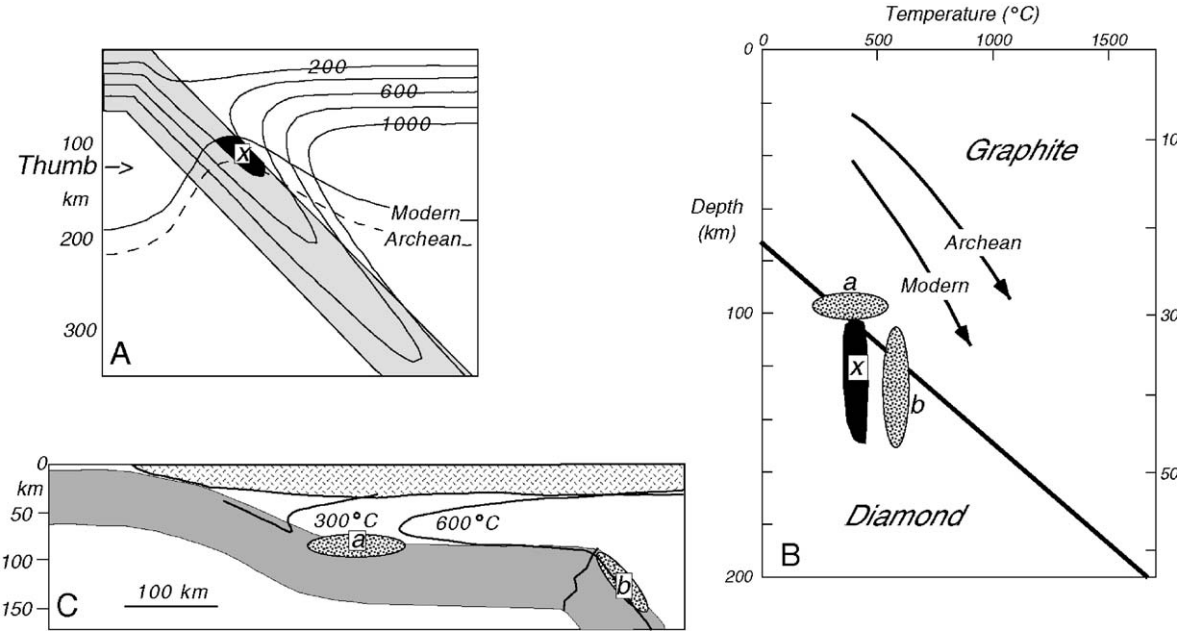

Fig. 10. Pressure–temperature constraints on diamond formation in an Archean subduction zone. A. Generalised subduction model showing a region of diamond stability in subducting slab, as inferred in the model of Griffin et al. (2000) for SE Australia. B. Idealised modern and Archean geothermal gradients (see Martin, 1986). Adapted from Griffin et al. (2000) with diamond–graphite transition boundary after Bundy et al. (1996). The field "x" illustrates the field of shallow diamond stability (in subducted slab) of Griffin et al. (2000). The fields "a" and "b" refer to the *P*–*T* domains marked in part C. C. The shallow subduction model of Gutscher et al. (2000), including a region of near-flat subduction, showing the approximate locations of two regions of diamond stability that encompass the top of the slab and overlying asthenosphere (a, b). As demonstrated by diamond-bearing peridotite massifs, diamond stability is not confined to the oceanic slab in subduction zone settings. In cases where subduction was at shallow angles, rather than the flat subduction considered here, the counterpart of diamond stability region "a" would occur at greater depths.

greater than 130 km, which exceed those implicated for the Thumb minette.

If many adakite slab melts result from shallow subduction, as suggested by Gutscher et al. (2000), then the presence of these rock types in the southern Superior Province provides an explanation for the occurrence of diamondiferous lamprophyres. Varying the angle of subduction, and therefore the location of the cold finger effect, allows for the creation of a lamprophyre-accessible diamond stability P–T window irrespective of the late Archean geotherm. The numerical modelling of Gutscher et al. (2000) illustrates that flat subduction initially heats up the slab causing it to melt at shallow depths. Importantly, melting will only occur for a few millions years and subduction quickly results in the cooling of asthenospheric mantle that can eliminate much of the convecting wedge. Whereas normal subduction may never have been able to stabilise diamonds at sites above the sources of Archean (or younger) lamprophyres, shallow angle subduction effectively creates a low-pressure diamond stability window over a wide temperature range. The low-P, low-T window is likely to extend from the subducting plate into the immediately overlying mantle. It must be noted, however, that the angle of subduction illustrated in Fig. 10C is based on the model of Gutscher et al. (2000) for parts of the Andes and the nearly horizontal slab it portrays represents an end member scenario (cf. Guillier et al., 2001). Where the angle of subduction is slightly greater then the diamond stability window will extend over a correspondingly larger pressure range.

The configuration of isotherms associated with the type of stepped slab illustrated in the Gutscher et al. (2000) model also allows for a second diamond stability window that, in terms of its P–T conditions, corresponds closely to the one generated by normal subduction. In contrast to normal subduction, however, the deeper stability window is closely associated with prominent curvatures in the slab and the subduction-generated perturbations of mantle isotherms.

When flat-lying oceanic crust begins to rollback and sink into the mantle during orogeny then heating of the frozen wedge and diamond source will initially be driven by adjacent subduction-modified asthenosphere that is a viable source for lamprophyric magmas. We suggest that sinking of the formerly flat slab will allow for the entrainment of at least one population of low-P, low-T diamonds by lamprophyres and perhaps multiple populations. This rollback scenario could account for the variable N systematics of Wawa diamonds reported by Stachel et al. (2004). Other differences in storage or entrainment histories of the diamonds cannot yet be ruled out. Computer-based "particle-in-cell finite-element modeling" of the shallow-angle subduction scenario is underway and should clarify these issues. Initial results support the inference that lamprophyric magmas have access to multiple diamond populations during the early phases of the slab rollback associated with orogeny (O'Neill and Wyman, 2005).

7. Conclusions

The occurrence of diamonds in Archean-aged shoshonitic lamprophyres provides important new insights into the tectonic events associated with orogeny and stabilisation of the Superior Province craton. The association of diamonds with comparatively rare breccias at both localities suggests that preservation of the carbon polymorphs may have been dependant upon transitory episodes of extreme crustal extension. The rapid magma ascent processes also favoured entrainment and preservation of xenoliths from the lithospheric mantle and was responsible for the high olivine content in many occurrences. In other respects, the diamond-hosting lamprophyre dikes and breccias are typical examples of shoshonitic lamprophyres, which have been associated with subduction-driven orogenies since the late Archean.

Based on analogies with younger counterparts, the majority of the deeply sourced xenoliths in the studied lamprophyres are websteritic cumulates generated by basaltic magma fractionation at the base of arc crust prior to orogeny. Trace element and isotopic data for the websterites record a metasomatic event in the lithosphere that created chemical heterogeneities, at the cm- to m-scale, prior to ascent of lamprophyric magma. The metasomatising fluid ($\varepsilon Nd_T \approx 8.5$) was LREE enriched but derived from an old LREE depleted source, possibly linked to the ~2.9 Ga Hawk assemblage that occurs near the Wawa diamond deposit. Unmetasomatised websterite and another xenolith have εNd_T of 4.2 and 2.9, at the time of lamprophyre emplacement, which suggests they are derived from the 2.7 Ga cycle of magmatism.

Entrainment of diamonds from the asthenospheric wedge or subducting plate by shoshonitic lamprophyres was probably rare at any time in the past, if orogeny followed normal subduction. In contrast, flat or shallow-angle subduction produces diamond stability windows at depths that are accessible to shoshonitic lamprophyres.

The diamond deposits of the Wawa and Abitibi Subprovinces provide important insights into orogeny at 2.7 Ga in the southern Superior Province and set out a number of important requirements that any tectonic model must address. These include a) a deep source for

oxidised metasomatic fluids that is activated prior to lamprophyre emplacement, b) a mechanism to isolate this isotopically aged and depleted source for 10s or 100s of Ma until it is heated in the mantle during orogeny, c) a hybridised mantle source for primitive, hydrous, shoshonitic lamprophyres, d) a sustained cold finger effect in the mantle to establish a shallow-mantle diamond stability window. A form of plate tectonics that closely resembles Phanerozoic plate subduction, albeit with a shallow subduction angle, most readily meets these requirements. Typically, events in the Archean mantle lithosphere, and the tectonic events that generated them, are obscured in samples that have been modified repeatedly over 2.7 billions years. For the first time, the diamonds, lamprophyres, and xenoliths provide firm constraints on the thermal regime of an Archean subduction zone and orogen, along with direct information about the character and fluid sources of individual hybridising events.

Acknowledgments

Band-Ore Resources Ltd and Prairie C Properties provided access to the deposit sites, unpublished reports and diamond samples. DW thanks Fiona Williams for early discussions on the diamond host rocks. JA thanks Ann Wilson, Gary Grabowski, and Christine Vaillancourt for geological tours, rock samples and lithogeochemical analyses from the Cobalt and Wawa areas. Denver Stone provided access to a pre-publication version of his manuscript and data. Julie Chartrand is thanked for drafting Fig. 1. The support for isotope analytical facilities and costs of Sm–Nd and Pb isotopic analyses were provided by LGI — Laboratório de Geologia Isotópica–UFRGS–Brazil. RC thanks Dr Edinei Koester for informative discussions and analytical assistance. Stephen Haggerty is thanked for many useful comments on an earlier version of the manuscript. Published with the permission of the Senior Manager of the Precambrian Geoscience Section of the Ontario Geological Survey. Thorough and constructive reviews by Z. Spetsius, S. Foley, and an anonymous reviewer greatly improved the final manuscript.

References

Armstrong, J.P., Barnett, R.L., 2003. The association of Zn-Chromite with diamondiferous lamprophyres and diamonds: unique compositions as a guide to the diamond potential of non-traditional diamond host rocks. 8th International Kimberlite Conference Extended Abstracts FLA_0230, 3 pages on Compact Disk.

Atherton, M.P., Ghani, A.A., 2002. Slab breakoff: a model for Caledonian, late Granite syn-collisional magmatism in the orthotectonic (metamorphic) zone of Scotland and Donegal, Ireland. Lithos 62, 65–78.

Ayer, J., Amelin, Y., Corfu, F., Kamo, S., Ketchum, J., Kwok, K., Trowell, N., 2002. Evolution of the southern Abitibi greenstone belt based on U–Pb geochronology: autochthonous volcanic construction followed by plutonism, regional deformation and sedimentation. Precambrian Research 115, 63–95.

Barron, L.M., Lishmund, S.R., Oakes, G.M., Barron, B.J., Sutherland, F.L., 1996. Subduction model for the origin of some diamonds in the Phanerozoic of eastern New South Wales. Australian Journal of Earth Sciences 43, 257–267.

Beccaluva, L., Bianchini, G., Bonadiman, C., Siena, F., Vaccaro, C., 2004. Coexisting anorogenic and subduction-related metasomatism in mantle xenoliths from the Betic Cordillera (southern Spain). Lithos 75, 67–87.

Bleeker, W., 2002. Archean tectonics: a review, with illustrations from the Slave Craton. In: Fowler, C.M.R., Ebinger, C.J., Hawkesworth, C.J. (Eds.), The Early Earth: Physical, Chemical and Biological Development.Geological Society of London Special Publication, vol. 199, pp. 151–181.

Brueckner, H.K., Carswell, D.A., Griffin, W.L., 2002. Paleozoic diamonds within a Precambrian peridotite lens in UHP gneisses of the Norwegian Caledonides. Earth and Planetary Science Letters 203, 805–816.

Bundy, F.P., Bassett, W.A., Weathers, M.S., Hemley, R.J., Mao, H.K., Goncharov, A.F., 1996. The pressure–temperature phase and transformation diagram for carbon; updated through 1994. Carbon 34, 141–153.

Cabo Mining Corporation (Vancouver) June 17, 2002, News release archived on the web at http://www.geocities.com/prairiec/newsarchive/archive.html.

Calvert, A.J., Ludden, J.N., 1999. Archean tectonic assembly in the southeastern Superior Province of Canada. Tectonics 18, 412–429.

Canning, J.C., Henney, P.J., Morrison, M.A., Gaskarth, J.W., 1996. Geochemistry of late Caledonian minettes from Northern Britain: implications for the Caledonian sub-continental lithospheric mantle. Mineralogical Magazine 60, 221–236.

Carmichael, I.S.E., Lange, R.A., Luhr, J.F., 1996. Quaternary minettes and associated volcanic rocks of Mascota, western Mexico: a consequence of plate extension above a subduction-modified mantle wedge. Contributions to Mineralogy and Petrology 124, 302–338.

Chopin, C., 2003. Ultrahigh-pressure metamorphism: tracing continental crust into the mantle. Earth and Planetary Science Letters 212, 1–14.

Conceição, R.V., Green, D.H., 2004. Derivation of potassic (shoshonitic) magmas by decompression melting of phlogopite+pargasite lherzolite. Lithos 72, 209–229.

Coogan, L.A., Banks, G.J., Gillis, K.M., MacLeod, C.J., Pearce, J.A., 2003. Hidden melt signatures in the Troodos ophiolite plutonic suite: evidence for widespread generation of depleted melts and intra-crustal melt aggregation. Contributions to Mineralogy and Petrology 144, 484–505.

Corfu, F., 1993. The evolution of the southern Abitibi greenstone belt in light of precise U–Pb geochronology. Economic Geology 88, 1323–1340.

Davies, G.R., Nixon, P.H., Pearson, D.G., Obata, M., 1993. Tectonic implications of graphitized diamonds from the Ronda peridotite massif, southern Spain. Geology 21, 471–474.

de Boorder, H., Spakman, W., White, S.H., Wortel, M.J.R., 1998. Late Cenozoic mineralization, orogenic collapse and slab detachment in

the European Alpine Belt. Earth and Planetary Science Letters 164, 569–575.
Ehrenberg, S.N., 1982. Petrogenesis of garnet lherezolite and megacrystalline nodules from the Thumb, Navajo volcanic field. Journal of Petrology 23, 507–547.
Feldstein, S.H., Lange, R., 1999. Pliocene potassic magmas from the Kings River region, Sierra Nevada, California: evidence for melting of a subduction-modified mantle. Journal of Petrology 40, 1301–1320.
Féménias, O., Coussaert, N., Bingen, Bernard, Whitehouse, M., Mercier, J.-C.C., Demaiffe, D., 2003. A Permian underplating event in late- to post-orogenic setting. Evidence from the mafic–ultramafic layered xenoliths of Beaunit (Franch Central Massif). Chemical Geology 199, 293–315.
Feng, R., Kerrich, R., 1992. Geochemical evolution of granitoids from the Archean Abitibi Southern Volcanic Zone and the Pontiac subprovince, Superior Province, Canada: implications for tectonic history and source regions. Chemical Geology 98, 23–70.
Fowler, M.B., Henney, P.J., 1996. Mixed Caledonian appinite magmas: implications for lamprophyre fractionation and high Ba–Sr granite genesis. Contributions to Mineralogy and Petrology 126, 199–215.
Garrido, C.J., Bodiner, J.-L., 1999. Diversity of mafic rocks in the Ronda peridotite: evidence for pervasive melt–rock interaction during heating of subcontinental lithosphere by upwelling asthenosphere. Journal of Petrology 40, 729–754.
Griffin, W.L., O'Reilly, S.Y., Davies, R.M., 2000. Subduction-related diamond deposits? Constraints, possibilities and new data from eastern Australia. Reviews in Economic Geology 11, 291–310.
Guillier, B., Chatelain, J.-L., Jallard, É., Yepes, H., Poupinet, G., Fels, J.F., 2001. Seismological evidence on the geometry of the orogenic system in central-northern Ecuador (South America). Geophysical Research Letters 28, 3749–3752.
Gutscher, M.A., Maury, R., Eissen, J.P., Bourdon, E., 2000. Can slab melting be caused by flat subduction? Geology 28, 535–538.
Helmstaedt, H.H., Doig, R., 1975. Eclogite nodules from kimberlite pipes of the Colorado Plateau; samples of subducted Franciscan-type oceanic lithosphere. Physics and Chemistry of the Earth 9, 95–111.
Herrmann, W., Berry, R.F., 2002. MINSQ—a least squares spreadsheet method for calculating mineral proportions from whole rock major element analyses. Geochemistry: Exploration, Environment, Analysis 2, 361–368.
Hofmann, A.W., 1997. Mantle geochemistry: the message from oceanic volcanism. Nature 385, 219–229.
Jacob, D.E., 2004. Nature and origin of eclogite xenoliths from kimberlites. Lithos 77, 295–316.
Kerrich, R., Wyman, D., 1990. Geodynamic setting of mesothermal gold deposits. An association with accretionary tectonic regimes. Geology 18, 882–885.
Laughlin, A.W., Charles, R.W., Shafiqullah, M., Husler, J., 1985. Tectonic implications of the age, composition and orientation of lamprophyre dykes, Navajo volcanic field, Arizona. Earth and Planetary Science Letters 76, 361–374.
Lefebvre, N., Kopylova, M., Kivi, K., Barnett, R., 2003. Diamondiferous volcaniclastic debris flow of Wawa, Ontario, Canada 8th International Kimberlite Conference Extended Abstracts FLA_0298, 3 pages on Compact Disk.
Liipo, J., Vuollo, J., Nykänen, V., Piirainen, T., Pekkarinen, L., Tuokko, I., 1995. Chromites from the early Proterozoic Outokumpu-Jormua Ophiolite Belt: a comparison with chromites from Mesozoic ophiolites. Lithos 36, 15–27.
Luhr, J.F., 1997. Extensional tectonics and the diverse primitive volcanic rocks in the Western Volcanic Belt. The Canadian Mineralogist 35, 473–500.
Machado, N., Brooks, C., Hart, S.R., 1986. Determination of initial $^{87}Sr/^{86}Sr$ and $^{143}Nd/^{144}Nd$ in primary minerals from mafic and ultramafic rocks: experimental procedure and implications for the isotopic characteristics of the Archean mantle under the Abitibi greenstone belt, Canada. Geochimica et Cosmochimica Acta 50, 2335–2348.
Martin, H., 1986. Effect of steeper Archean geothermal gradient on geochemistry of subduction-zone magmas. Geology 14, 753–756.
Mazzucchelli, M., Rivalenti, G., Vannucci, R., Bottazzi, P., Ottolini, L., Hofmann, A.W., Parenti, M., 1992. Primary positive Eu anomaly in clinopyroxene of low-crust gabbroic rocks. Geochimica et Cosmochimica Acta 56, 2363–2370.
McCuaig, T.C., Kerrich, R., 1998. *P–T–t*-deformation–fluid characteristics of lode gold deposits: evidence from alteration systematics. Ore Geology Reviews 12, 381–453.
McDonough, W.F., Sun, S.S., 1995. The composition of the Earth. Chemical Geology 120, 223–253.
McInnes, B.I.A., Gregoire, M., Binns, R.A., Herzig, P.M., Hannington, M.D., 2001. Hydrous metasomatism of oceanic sub-arc mantle, Lihir, Papua New Guinea: petrology and geochemistry of fluid metasomatised mantle wedge xenoliths. Earth and Planetary Science Letters 188, 169–183.
Mitchell, R.H., Bergman, S.C., 1991. Petrology of Lamproites. Plenum Press, New York. 447 pp.
Morrison, M.A., Hendry, G.L., Leat, P.T., 1987. Regional and tectonic implications of parallel Calaedonian and Permo-Carboniferous lamprophyre dyke swarms from Lismore, Ardgour. Transactions of the Royal Society of Edinburgh. Earth Sciences 77, 279–288.
Muir, T.L., 1997. Hemlo gold deposit area. Ontario Geological Survey Report 289. 219 pp.
Nagler, T.F., Kramers, J.D., 1998. Nd isotopic evolution of the upper mantle during the Precambrian: models, data and the uncertainty of both. Precambrian Research 91, 233–252.
O'Brien, P.J.O., Rötzler, J., 2003. High-pressure granulites: formation, recovery of peak conditions and implications for tectonics. Journal of Metamorphic Petrology 21, 3–20.
O'Neill, C., Wyman, D.A., 2005. Geodynamic modeling of late Archean subduction: *P–T* constraints from greenstone belt diamond deposits. In: Benn, K., Mareschal, J.-C., Condie, K. (Eds.), American Geophysical Union Monograph 164, Archean Geodynamics and Environments, pp. 177–188.
Parlak, O., Höck, V., Delaloye, M., 2002. The supra-subduction zone Pozanti-Karsanti ophiolite, southern Turkey: evidence for high-pressure crystal fractionation of ultramafic xenoliths. Lithos 65, 205–224.
Pearson, D.G., Davies, G.R., Nixon, P.H., 1993. Geochemical constraints on the petrogenesis of diamond facies pyroxenites from Beni Bousera peridotite massif, north Morocco; derivation from subducted oceanic lithosphere. Earth and Planetary Science Letters 102, 289–301.
Percival, J.A., Stern, R.A., Skulski, T., Card, K.D., Mortensen, J.K., Bégin, N.J., 1994. Minto Block, Superior Province: missing link in deciphering assembly of the craton at 2.7 Ga. Geology 22, 839–842.
Perring, C.S., Rock, N.M.S., Golding, S.D., Roberts, D.E., 1989. Criteria for the recognition of metamorphosed lamprophyres: a

case study from the Archaean of Kambalda, western Australia. Precambrian Research 43, 215–237.
Righter, K., Carmichael, I.S.E., 1996. Phase equilibria of phlogopite lamprophyres from Western Mexico: biotite-liquid equilibria and *P–T* estimates for biotite-bearing igneous rocks. Contributions to Mineralogy and Petrology 123, 1–21.
Riter, J.C.A., Smith, D., 1996. Xenolith constraints on the thermal history of the mantle below the Colorado Plateau. Geology 24, 267–270.
Rock, N.M.S., 1984. Nature and origin of "calc-alkaline lamprophyres" minettes, vogesites, kersantites and spessartites. Transactions of the Royal Society of Edinburgh. Earth Sciences 74, 193–227.
Rock, N.M.S., 1991. Lamprophyres. Blackie and Son Ltd., Glasgow. 285 pp.
Roden, M.F., Shimizu, N., 2000. Trace element abundances in mantle-derived minerals which bear on compositional complexities in the lithosphere of the Colorado Plateau. Chemical Geology 165, 283–305.
Rogers, N.W., Bachinski, S.W., Henderson, P., Parry, S.J., 1982. Origin of potash-rich basic lamprophyres: trace element data for Arizona minettes. Earth and Planetary Sciences Letters 57, 305–312.
Saccani, E., Photiades, A., 2004. Mid-ocean ridge and suprasubduction affinities in the Pindos ophiolites (Greece): implications for magma genesis in a forearc setting. Lithos 73, 229–253.
Sage, R.P., 1994. Geology of the Michipicoten greenstone belt. Ontario Geological Survey Open File Report, vol. 5888. 435 pp.
Sage, R.P., 2000. The "Sandor" diamond occurrence, Michipicoten Greenstone Belt, Wawa, Ontario: a preliminary study. Ontario Geological Survey Open File Report, vol. 6016. 49 pp.
Schiller, E., 2003. Wawa diamonds. Resource World Magazine, pp. 21–25 (June).
Shand, P., Gaskarth, J.W., Thirlwall, M.F., Rock, N.M.S., 1994. Late Caledonian lamprophyre dyke swarms of south-eastern Scotland. Mineralogy and Petrology 51, 277–298.
Sharma, M., Wasserburg, G.J., Papanastassiou, D.A., Quick, J.E., Sharkov, E.V., Laz'ko, E.E., 1995. High $^{143}Nd/^{144}Nd$ in extremely depleted mantle rocks. Earth and Planetary Science Letters 135, 101–114.
Shirey, S.B., Hanson, G.N., 1986. Mantle heterogeneity and crustal recycling in Archean granite–greenstone belts: evidence from Nd isotopes and trace elements in the Rainy Lake area, Superior Province, Ontario, Canada. Geochimica et Cosmochimica Acta 50, 2631–2651.
Smith, D., 1995. Chlorite-rich ultramafic reaction zones in Colorado Plateau xenoliths: recorders of sub-Moho hydration. Contributions to Mineralogy and Petrology 121, 185–200.
Smith, D., Griffin, W.L., Ryan, C.G., Sie, S.H., 1991. Trace-element zonation in garnets from the Thumb: heating and melt infiltration below the Colorado Plateau. Contributions to Mineralogy and Petrology 107, 60–79.
Smith, D., Riter, J.C.A., Mertzman, S.A., 1999. Erratum to "Water–rock interactions, orthopyroxene growth, and Si-enrichment in the mantle: evidence in xenoliths from the Colorado Plateau, southwestern United States" [Earth Planet. Sci. Lett. 165 (1999) 45–54]. Earth and Planetary Science Letters 167, 347–356.
Smithies, R.K., 2000. The Archaean tonalite–trondhejemite–granodiorite (TTG) series is not an analogue of Cenozoic adakite. Earth and Planetary Science Letters 182, 115–125.
Stone, D., Semenyna, L., 2004. Petrography, chemistry and diamond characteristics of heterolithic breccia and lamprophyre dikes at Wawa, Ontario. Ontario Geological Survey, Open File Report, vol. 6134. 39 pp.
Stachel, T., Blackburn, L., Kuzlaukis, S., Barton, E., Walker, E.C., 2004. Diamonds from the Cristal and Genesis Volcanics, Wawa area, Ontario. Abstract. Proceedings of the 32th Annual Yellowknife Geoscience Forum. November 2004, Yellowknife, Canada.
Stott, G.M., Ayer, J.A., Wilson, A.C., Grabowski, G.P.B., 2002. Are the Neoarchean diamond-bearing breccias in the Wawa area related to late-orogenic alkalic and "sanukitoid" intrusions? Summary of Field Work and Other Activities 2002, Ontario Geological Survey, Open File Report 6100, 9-1 –9-10.
Thorpe, R.I., 1999. The Pb isotope linear array for volcanogenic massive sulfide deposits of the Abitibi and Wawa Subprovinces, Canadian Shield. Economic Geology Monographs 10, 555–576.
Tomlinson, K.Y., Bowins, R., Heshler, J., 1998. Refinement of Hafnium (Hf) and Zirconium (Zr) ICP_MS analysis by improvement in sample digestion procedure. Summary of fieldwork and other activities 1998. Ontario Geological Survey Miscellaneous Paper 169, 189–192.
Turek, A., Sage, R.P., Van-Schmus, W.R., 1992. Advances in the U–Pb zircon geochronology of the Michipicoten greenstone belt, Superior Province, Ontario. Canadian Journal of Earth Sciences 29, 1154–1165.
Vaillancourt, C., Ayer, J.A., Zubowski, S.M, Kamo, S.L., 2004. Synthesis and timing of Archean geology and diamond-bearing rocks in the Michipicoten greenstone belt: Menzies and Musquash Townships. Summary of field work and other activities 2004, Ontario Geological Survey Open File Report 6145, 6-1 to 6-9.
Vaillancourt, C., Ayer, J.A., Hamilton, M.A., 2005. Synthesis of Archean geology and diamond-bearing rocks in the Michipicoten greenstone belt: results from microdiamond extraction and geochronological analysis. Summary of Field Work and Other Activities 2005, Ontario Geological Survey Open File Report 6172, 8-1–8-13.
Vaniman, D., Laughlin, A.W., Gladney, E.S., 1985. Navajo minettes in the Cerros de las Mujeres, New Mexico. Earth and Planetary Science Letters 74, 69–80.
van Roermund, H.L.M., 2002. Microdiamonds in a megacrystic garnet websterite pod from Bardane on the island of Fjortoft, western Norway: evidence for diamond formation in mantle rocks during deep continental subduction. Geology 30, 959–962.
Velde, D., 1968. Les transformations de l'olivine dans les lamprophyres et lamproites. Bulletin de la Société Géologique de France 10, 601–612.
Williams, F., 2002. Diamonds in late Archean calc-alkaline lamprophyres Ontario, Canada: origins and implications. Honours Thesis unpublished, University of Sydney, 82p.
Williams, H.R., Stott, G.M., Heather, K.B., Muir, T.L., Sage, R.P., 1991. Wawa Subprovince. Geology of Ontario. Ontario Geological Survey, Special, vol. 4, Part 1, pp. 485–539.
White, D.J., Musacchio, G., Helmstaedt, H.H., Harrap, R.M., Thurston, P.C., van der Velden, A., Hall, K., 2003. Images of a lower-crustal oceanic slab: direct evidence for tectonic accretion in the Archean western Superior province. Geology 31, 997–1000.
Wortel, M.J.R., Sparkman, W., 2000. Subduction and slab detachment in the Mediterranean–Carpathian region. Science 290, 1910–1917.
Wyman, D.A., Kerrich, R., 1988. Alkaline magmatism, major structures, and gold deposits: implications for greenstone belt gold metallogeny. Economic Geology 83, 454–461.
Wyman, D.A., Kerrich, R., 1989. Archean shoshonitic lamprophyres of the Superior Province, Canada: distribution, petrology and

geochemical characteristics. Journal of Geophysical Research 94B, 4667–4696.

Wyman, D.A., Kerrich, R., 1993. Archean shoshonitic lamprophyres of the Abitibi subprovince, Canada: petrogenesis, age, and tectonic setting. Journal of Petrology 34, 1067–1109.

Wyman, D.A., Bleeker, W., Kerrich, R., 1999. A 2.7 Ga plume, proto-arc, to arc transition and the geodynamic setting of the Kidd Creek deposit: evidence from precise ICP MS trace element data. Economic Geology Monographs 10, 511–528.

Wyman, D.A., Kerrich, R., Polat, A., 2002. Assembly of archean cratonic mantle lithosphere and crust: plume-arc interaction in the Abitibi–Wawa subduction–accretion complex. Precambrian Research 115, 37–62.